Solid State Sciences 151 (2024) 107526

Contents lists available at ScienceDirect

Solid State Sciences

journal homepage: www.elsevier.com/locate/ssscie

Thermally stable and red emitting bismuth ions sensitized $SrGa_2O_4:Eu^{3+}$ phosphors for phosphor converted WLED applications

B. Vasanthi [a,b], N. Gopakumar [b], P.S. Anjana [a,*]

[a] Post Graduate Department of Physics, All Saints' College, University of Kerala, Thiruvananthapuram, Kerala, 695007, India

[b] Post Graduate Department of Physics and Research Centre, Mahatma Gandhi College, University of Kerala, Thiruvananthapuram, Kerala, 695004, India

ARTICLE INFO

Keywords:
Phosphor
X-ray diffraction
Photoluminescence
Temperature dependent photoluminescence
Mechanoluminescence

ABSTRACT

A series of Bi^{3+} sensitized $SrGa_2O_4:0.08Eu^{3+}$ phosphors have been synthesized by high temperature solid-state reaction method. The structural and surface morphological studies have been characterized by X-ray diffraction, Field emission scanning electron microscopy and Energy dispersive X-ray analysis. The optical and luminescence properties of phosphors are done using UV–Visible absorption spectroscopy, photoluminescence excitation and emission spectra and mechanoluminescence studies. X-ray diffraction analysis shows that the phosphors are single phase with monoclinic structure. The intensity of prominent red emission enhanced with the incorporation of Bi^{3+} ions in $SrGa_2O_4:0.08Eu^{3+}$ phosphors due to the effective energy transfer between Bi^{3+} and Eu^{3+} ions. The optimized $SrGa_2O_4:0.08Eu^{3+},0.05Bi^{3+}$ phosphor has excellent thermal stability about 96.7% with an activation energy of 0.253 eV. These phosphors can exhibit better mechanoluminescence properties without any irradiation. The synthesized phosphors can be used in solid state lighting, phosphor converted white light emitting diodes and stress sensing applications etc.

1. Introduction

Spinel-structured phosphors are more attractive than other types of phosphors due to their superior optical and luminescence qualities, good radiation damage resistance, high temperature and chemical stability. The spinel has general crystal formula AB_2O_4 (A = Zn, Mg, Ba, Ca, Sr, B═Ga, Al) where A and B are divalent and trivalent metallic cations respectively [1–3]. $SrGa_2O_4$ is one of the phases of $SrO–Ga_2O_3$ combinations and other phases are $SrGa_{12}O_{19}$, $SrGa_4O_7$, $Sr_3Ga_4O_9$, $Sr_3Ga_2O_6$, $Sr_{10}Ga_6O_{19}$ and $Sr_4Ga_2O_7$ respectively [4–6]. It is well known that introducing different rare earth ions into host materials can emit different colors ascribed to 4f- 4f or 4f-5d transitions [7]. Eu^{3+} ion is one such dopant which provides excellent luminescence properties in host matrix. Eu^{3+} ion has been playing a significant role in modern red lighting, fluorescent lamps, luminescent probe and other optoelectronic devices owing to its characteristic emissions originating from the transitions of $^5D_0 \rightarrow {}^7F_J$ (J = 0, 1, 2, 3, 4) [8]. The photoluminescence emission spectrum comprises narrow and intense lines in the red region, the energies of which are practically independent of the host lattice [9]. The role of co-dopant ions in different host matrices has a wide attention in the enhancement of luminescence emission. Hence Bi^{3+} ions in Eu^{3+} activated phosphors become key role in research field for the enhancement of luminescence efficiency [10]. Bi^{3+} ions are non-rare earth element and it can act as an activator and a sensitizer in many rare earth, non-rare earth and transition metals activated host matrices [11]. Bi^{3+} ions have grown to be a well-known sensitizer due to their special characteristics like diverse oxidation states and ability to exhibit wide range of luminescence emission colors etc due to their naked 6s electrons that arise from an electronic configuration of $[Xe]4f^{14}5d^{10}6s^2$ [12]. It can enhance the emission intensity by means of effective energy transfer between Bi^{3+} and activator ions in host phosphors. Bi^{3+} ion emerged as an important sensitizer especially in the case of Eu^{3+} ions and wide applications based on such combinations have been reported [13]. It can enhance the luminescence emission of Eu^{3+} ions doped phosphors due to the overlapping of emission band of Bi^{3+} in the range of 380–600 nm with the partial excitation region of Eu^{3+} ions [10]. Such phosphors exhibit excellent red luminescence attributed by this energy transfer mechanism between $Bi^{3+} \rightarrow Eu^{3+}$ ions. Bismuth ions possess different valence states and it can show luminescence emission colors such as blue, green and yellow in the visible spectrum due to the $^3P_1 \rightarrow {}^1S_0$ and $^1P_1 \rightarrow {}^1S_0$ transitions respectively. It indicates the color tunability behavior with different host materials [12].

* Corresponding author.
E-mail addresses: vasanthi.b.1991@gmail.com (B. Vasanthi), gopkumar.n@gmail.com (N. Gopakumar), psanjanaa@yahoo.com (P.S. Anjana).

https://doi.org/10.1016/j.solidstatesciences.2024.107526
Received 7 January 2024; Received in revised form 24 March 2024; Accepted 25 March 2024
Available online 28 March 2024

Mechanoluminescent (ML) materials attracts the research field due to its immense applications in damage sensors, fracture sensors, stress detectors, earth quake detectors, biomedicine etc. owing to its wireless, non-destructive, reproducible and reliable stress sensing properties [7]. The sources which produce mechanoluminescence include rubbing, cutting, friction, impact, deformation, stress, vibration etc. Depending upon these parameters, there are different categories of ML [14,15]. In this process mechanical energy is converted into light energy. The mechanoluminescence from strontium aluminate based systems doped with different activator ions have been widely discussed in literature [16,17]. The ML studies of gallate based phosphors are rarely reported.

The Eu^{3+} doped $SrGa_2O_4$ phosphors exhibited red emission with better color characteristics and thermal stability and hence it can be an essential component in phosphor-converted white light emitting diodes [18]. In this work an attempt has been made to investigate the role of Bi^{3+} ions as sensitizers for improving thermal stability and color characteristics of red emission of Eu^{3+} doped $SrGa_2O_4$ phosphors. The structural, morphological, optical, and luminescence studies of Bi^{3+}co-doped in Eu^{3+} activated $SrGa_2O_4$ phosphors has been investigated. The variations in the ML glow curve intensity with different Bi^{3+} concentrations and impact velocity have been studied. The synthesized phosphors exhibit mechanoluminescence properties without any pre irradiation is one of the credits of our work.

To the best of our knowledge, the photoluminescence and mechanoluminescence properties of Eu^{3+}, Bi^{3+} co-doped $SrGa_2O_4$ phosphors has not been investigated. The structure and luminescence properties of spinel gallate phosphors co-doped with Bi^{3+} and Eu^{3+} ions have rarely been reported. Zhengwen Yang et al. (2013) discussed the photoluminescence characteristics and energy transfer of $ZnGa_2O_4$ phosphors co-doped with Bi^{3+} and Eu^{3+} ions [19]. Rong Ying Liu et al. (2015) reported the effect of Bi^{3+} on luminescent properties of $Sr_{3-x}GaO_4F$: xEu^{3+} phosphors [20]. Tsiumra et al. (2019) reported the crystal structure and photoluminescence studies of the Bi^{3+} and Bi^{3+}- Eu^{3+} co-doped $Gd_3Ga_5O_{12}$ phosphors [21]. Liang Zhang et al. (2021) focused on the site occupancy preference of Bi^{3+} and Bi^{3+}– Eu^{3+} co-doped Y_3GaO_6 phosphors for white LEDs [22]. Zheng Lu et al. (2023) studied the new color-tunable $LaCaGaO_4$:Bi^{3+}, Eu^{3+} phosphors for warm white LEDs with better color rendering properties [23]. The synthesized phosphors in the present study can provide insight into the Bi^{3+} ion as a sensitizer to improve the luminescence properties of the Eu^{3+} activated strontium gallate phosphors. The present work suggests that the synthesized $SrGa_2O_4$:Eu^{3+}, Bi^{3+} phosphors can serve as a suitable red emitter in phosphor converted WLEDs, solid state light emitting devices, sensors and stress indicators.

2. Experimental techniques

2.1. Sample preparation

$SrGa_2O_4$:0.08 Eu^{3+}, yBi^{3+} (y = 0, 0.02, 0.05, 0.08, 0.1) phosphors were synthesized by conventional high temperature solid-state reaction method. The co-dopant concentration of the Bi^{3+} ion is changed and the molar concentration of the Eu^{3+} ion is fixed at 8 mol % (x = 0.08). The stoichiometric amounts of $SrCO_3$ (99.6%, Sigma Aldrich), Ga_2O_3 (99.99%, Alfa Aesar), Eu_2O_3 (99.99%, Alfa Aesar), and Bi_2O_3 (Sigma Aldrich, 99.9% purity) were used as starting materials. The required stoichiometric amounts of these raw materials were weighed accurately and then thoroughly mixed in an agate mortar and pestle with distilled water as the medium for 2 h. It is then dried in an oven and then transferred into a platinum crucible and calcined at optimum temperature of 1250° C for 5 h at a heating rate of 10 °C/min. The calcined powder is then ground for characterization. The composition and sample codes of the synthesized phosphors are tabulated in Table 1.

Table 1
The composition and sample codes for the Bi^{3+} co-doped $SrGa_2O_4$:0.08 Eu^{3+} phosphors.

Phosphor	Sample code
$SrGa_2O_4$	SGO
$SrGa_2O_4$:0.08 Eu^{3+}	SGEu:0.08
$SrGa_2O_4$:0.08 Eu^{3+}, 0.02 Bi^{3+}	SGEBi:0.02
$SrGa_2O_4$:0.08 Eu^{3+}, 0.04Bi^{3+}	SGEBi:0.04
$SrGa_2O_4$:0.08 Eu^{3+}, 0.05 Bi^{3+}	SGEBi:0.05
$SrGa_2O_4$:0.08 Eu^{3+}, 0.08 Bi^{3+}	SGEBi:0.08
$SrGa_2O_4$:0.08 Eu^{3+}, 0.1 Bi^{3+}	SGEBi:0.1

2.2. Powder characterization

The phase identification of the synthesized phosphors was done with X-ray diffraction (XRD) technique on powder samples using a Bruker AXS D8 Advanced X-ray diffractometer. The pattern was collected over 2ɵ ranging from 10 to 80° with a step size of 0.01° at scanning rate of 4.0°/min using CuKα radiation (λ = 1.54 Å). The microstructure and surface morphology of the prepared phosphors were analyzed using Nova NanoSEM 450 UoK Field Emission Scanning Electron Microscope (FESEM). Energy dispersive X-ray analysis (EDAX) is carried out using Carl Zeiss EVO 18 Research instrument. The regions of absorption and band gap energy of the prepared phosphors were determined from UV–Visible studies using PerkinElmer UV/VIS/NIR Spectrometer Lamda 950 in the range 200–800 nm. Photoluminescence excitation (PL) and emission characteristics were investigated by a Fluorescence spectrophotometer (Fluorolog Horiba) equipped with a 150 W xenon lamp as excitation source. The color coordinates of the phosphors were also calculated using 1931 CIE chromaticity software. The decay profiles of the phosphors were recorded using EDINBURGH FLS 1000 under the excitation of 394 nm and emission wavelength of 616 nm. Using a home-made heater setup, the temperature-dependent photoluminescence (TDPL) response of the optimized phosphor was measured from 23 °C to 210 °C using a Hitachi 650–40 Fluorescence spectrophotometer. The Mechanoluminescence (ML) emission from the doped phosphors without any pre-irradiation of UV or gamma rays were monitored by an indigenous set up having photomultiplier tube (PMT 931A) positioned below the Lucite plate and connected to a digital storage oscilloscope. ML was excited by hitting a load of mass 100 g on to the doped phosphor from different heights using a guiding cylinder. The impact velocity was calculated using the equation $(2gh)^{1/2}$.

3. Results and discussion

3.1. X-ray diffraction (XRD)

. The XRD patterns of $Sr_{(1-x-y)}Ga_2O_4$: 0.08Eu^{3+}, yBi^{3+} (y = 0.02, 0.05, 0.08, 0.10) phosphors are shown in Fig. 1. The XRD patterns of Bi^{3+} co-doped $SrGa_2O_4$:0.08 Eu^{3+} phosphors are consistent with the standard ICDD card no. (01-070-5915) of host. Bi^{3+} co-doped phosphors are single phase with monoclinic crystal structure. The lattice parameters of host $SrGa_2O_4$ ceramic are a = 8.3770(3) Å, b = 8.9940(2) Å and c = 10.6800(4) Å. The effective ionic radii of Sr^{2+}, Ga^{3+}, Eu^{3+} and Bi^{3+} are 1.13, 0.62, 1.07 and 1.11 Å respectively [18,24]. The comparison of the ionic radii show that Eu^{3+} and Bi^{3+} ions can occupy the site of Sr^{2+} ions in the host lattice. The co-doping of Bi^{3+} ions into the $SrGa_2O_4$:0.08 Eu^{3+} phosphors do not cause any remarkable changes in the peak positions as well as crystal structure of the host matrix [25–27]. This result proves the successful doping and co-doping of Eu^{3+} and Bi^{3+} ions into the host lattice [26]. Hence the phase purity of these series of phosphors is verified [27]. The prominent peaks in the XRD patterns correspond to (−112), (−113), (131), (−311), (410), (034) and (224) planes of the host itself.

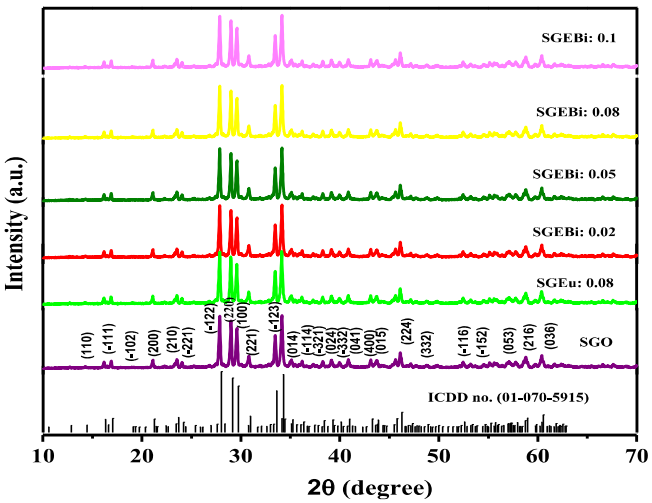

Fig. 1. XRD patterns of $Sr_{(1-x-y)}Ga_2O_4$: xEu^{3+}, yBi^{3+} (y = 0.02, 0.05, 0.08, 0.1) phosphors.

3.2. Morphology studies

3.2.1. Field emission scanning electron microscopy (FESEM)

Fig. 2(a-d) elucidates the FESEM micrographs of undoped and $SrGa_2O_4$:0.08 Eu^{3+}, yBi^{3+} (y = 0, 0.05, 0.1) phosphors. For undoped $SrGa_2O_4$ phosphor, the particles are slightly aggregated with irregular shapes and its sizes ranging from 1 to 3 μm. In the case of Eu^{3+} doped and Bi^{3+} co-doped $SrGa_2O_4$ phosphors, the particles are exist in aggregates form with different shapes and its sizes ranging from 1 to 5 μm. It is noticed that the particles sizes are nearly same for different concentrations of Bi^{3+} ions. The results show that the incorporation of Eu^{3+} and Bi^{3+} ions does not make significant changes to the morphology and size of the phosphors [16,18].

3.2.2. Energy dispersive X - ray spectroscopy (EDAX)

The EDAX analysis of undoped and $Sr_{(1-x-y)}Ga_2O_4$: $0.08Eu^{3+}$, yBi^{3+} (y = 0, 0.05) phosphors are shown in Fig. 3 (a-b). The peaks in the EDAX spectrum shows that Sr, Ga, O, Eu and Bi ions are completely incorporated and homogeneously distributed throughout the synthesized phosphors [18,28]. The weight percentage of Bi^{3+} ion is less than Eu^{3+} ion and is evident from EDAX spectrum.

3.3. UV–visible absorption spectra

Fig. 4(a) represents the absorption spectra of $Sr_{(1-x-y)}Ga_2O_4$: $0.08Eu^{3+}$, yBi^{3+} (y = 0.02, 0.05, 0.08, 0.1) phosphors. The bands recorded at 225 and 252 nm are ascribed to the charge transfer state of host and charge transfer band of $O^{2-} \rightarrow Eu^{3+}$ ions respectively [29]. The absorption bands between 285 and 310 nm are attributed to the transition of Bi^{3+} ions from $^1S_0 \rightarrow {}^1P_1$ transitions respectively. The band at 252 nm overlaps with those at 285 and 303 nm corresponds to the $^1S_0 \rightarrow {}^1P_1$ transition of Bi^{3+} ion and it is marked in the circle given in the graph. The absorption in the range 300–350 nm is attributed to $^1S_0 \rightarrow {}^3P_1$ transition of Bi^{3+} ions [12,13]. After co-doping with Bi^{3+} ions, the charge transfer band broadens but the band obtained between 200 and 300 nm are unaltered [29–31]. The inset of Fig. 4(a) displays the characteristic absorption bands of Eu^{3+} ions in the 350–550 nm range. These bands are recorded at 365, 371, 384, 395, 413, and 465 nm correspond to the following ($^7F_0 \rightarrow {}^5D_4$), ($^7F_0 \rightarrow {}^5L_8$), ($^7F_0 \rightarrow {}^5G_2$), ($^7F_0 \rightarrow {}^5L_6$), ($^7F_0 \rightarrow {}^5D_3$) and ($^7F_0 \rightarrow {}^5D_2$) transitions of Eu^{3+} ions respectively [27–31]. In the case of Eu^{3+} doped phosphor an additional absorption broad in the region of 350–400 nm centered at 374 nm is due to $^7F_0 \rightarrow {}^5L_8$ transition of Eu^{3+} ion. Ekta Rai et al. (2020) reported the presence of such band at 376 nm in the case of Eu^{3+} singly doped $LaVO_4$ phosphors

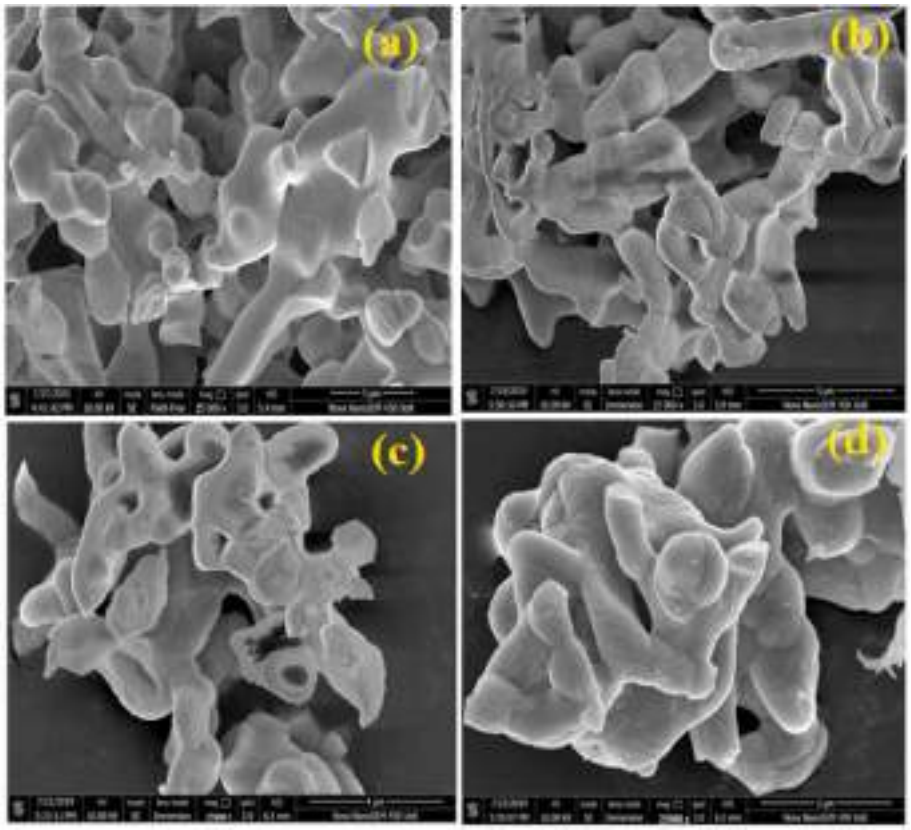

Fig. 2. FESEM micrographs of **(a)** undoped **(b)** $SrGa_2O_4$:0.08 Eu^{3+} **(c–d)** $SrGa_2O_4$:$0.08Eu^{3+}$, yBi^{3+} (y = 0.05, 0.1) phosphors.

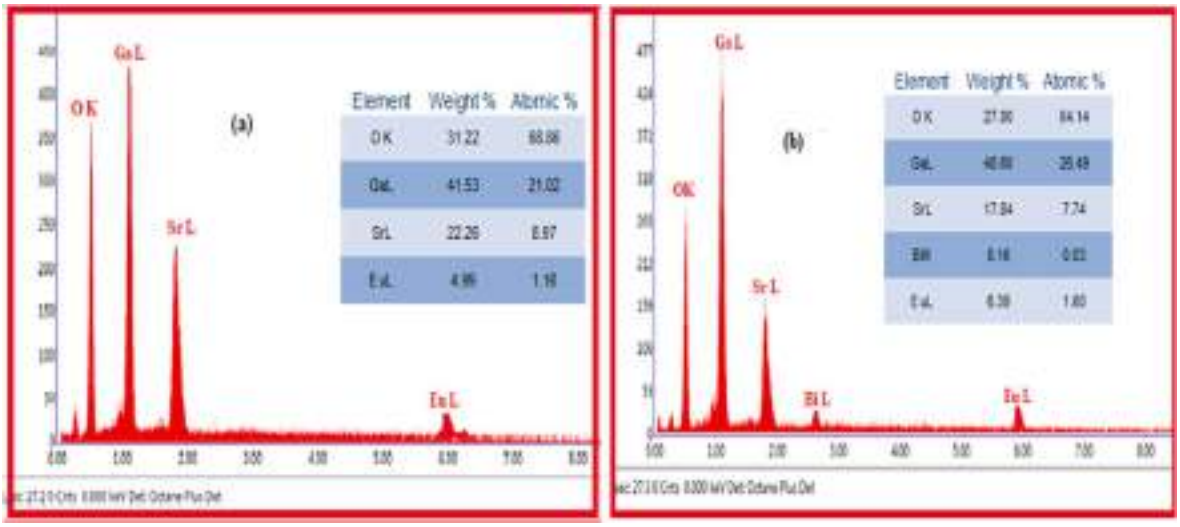

Fig. 3. EDAX spectrum of **(a)** $SrGa_2O_4$: 0.08 Eu^{3+} **(b)** $SrGa_2O_4$:0.08Eu^{3+}, 0.05Bi^{3+} phosphors.

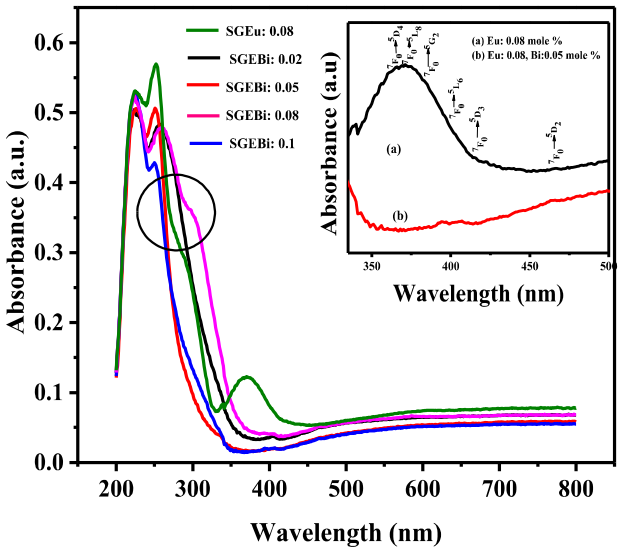

Fig. 4(a). Absorption spectra of $Sr_{(1-x-y)}Ga_2O_4$: xEu^{3+}, yBi^{3+} (x = 0.08, y = 0.02, 0.05, 0.08, 0.1) phosphors (Inset shows the absorption region between 350 and 500 nm).

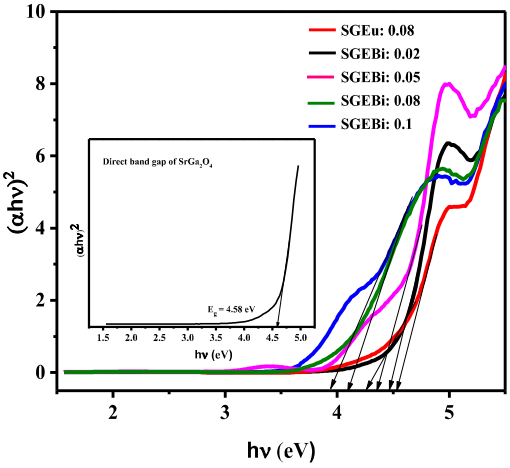

Fig. 4(b). Direct Band gap of $Sr_{(1-x-y)}Ga_2O_4$:xEu^{3+}, yBi^{3+} (x = 0.08, y = 0.02, 0.05, 0.08, 0.1) phosphors.

and absence of that band in Bi^{3+} sensitized phosphors. The intensity of broad band span from 340 to 420 nm with maximum at 374 nm decreases and transferred its absorbed energy to the peaks in the range of 340–420 nm [28]. The excitation region of bismuth ion lies in the range of 300–400 nm. Except that band, the absorption spectrum of Eu^{3+} doped as well as Bi^{3+} co-doped phosphors exhibit almost similar patterns. As Bi^{3+} concentration rises, the absorption changes towards the higher-wavelength region [32]. This results from the change in impurity level caused by the co-doping of Bi^{3+} with the conduction band. Thus, it is expected that the phosphors can be activated successfully in both the UV and visible regions [28,29]. The absorption spectrum of Eu^{3+} singly doped as well as Bi^{3+} co-doped phosphors exhibit almost similar patterns [20,32].

The tauc's plot of $SrGa_2O_4$ and $SrGa_2O_4$:0.08 Eu^{3+}, yBi^{3+} (y = 0, 0.02, 0.05, 0.08, 0.1) phosphors are shown in Fig. 4(b). The energy band gap of these phosphors are calculated from tauc's plot using the equation

$$(\alpha\, h\nu)^{1/n} = c\left(h\nu\text{-}E_g\right) \quad (1)$$

where α is the absorption coefficient, hν is the photon energy. If the value of n = 1/2, then it is allowed direct transition and n = 2 is for allowed indirect transition. The optical band gap is calculated by extrapolating the linear portion of the curve to $(\alpha h\nu)^2 = 0$ of $(\alpha h\nu)^2$ versus hν graph [17,30]. $SrGa_2O_4$ is a wide band gap semi-conducting material with band gap about 4.58 eV (inset of Fig. 4(b)). The Ga^{3+} ions combine with UV-generated free electrons to produce oxygen vacancies [18]. The luminescence in $SrGa_2O_4$ phosphors is arising from the presence of Ga^{3+} ions, which act as the luminescence centre in the material. Ga^{3+} ions are situated in the center of Ga–O tetrahedrons [26]. This luminescence centre can receive excitation energy through direct excitation or through energy transfer between adjacent ions. The electronic configuration of Ga^{3+} is 3 d^{10} and it is completely filled. Ga^{3+} ions are excited, one electron in the 3d orbital will be excited to the 4s orbital [25]. Electrons transition from the ground states to the excited state takes place due to the energy transfer from nearby Ga^{3+} ions to Ga–O polyhedra. These Ga–O tetrahedrons are excited by the UV light, electrons move from 2p orbital of O^{2-} to 4s orbital of Ga^{3+} ions. Following this, radiation transitions from the 4s orbital return the electrons to the 3d orbital, resulting in the formation of light. The four O^{2-} ions are

situated on the outside of the Ga–O tetrahedrons [25,26]. This makes it easier to excite the outer O^{2-} ions. Occurrences of oxygen vacancies are always present on the surfaces of the β-Ga_2O_3 crystal planes and exert a significant influence on its optical and luminescence properties. Oxygen atoms have the ability to leave lattice positions and create vacancies at high temperatures [26].

The band gap energy of $SrGa_2O_4$:0.08 Eu^{3+} phosphor is calculated to be 4.52 eV [14,18]. When europium ion is introduced into $SrGa_2O_4$ phosphor, charge transfer band from 2p orbit of O^{2-} to 4f orbit of Eu^{3+} ion take place. There is a formation of extra levels in the band gap between conduction and valence band. If the doping density is high, Eu^{3+} states generate a band. If this band is very nearer to conduction band edge, the band-gap will decrease [18]. As the co-doping concentration of Bi^{3+} ions increases, the band gap energies decrease and its values are 4.47, 4.38, 4.25 and 3.98 eV respectively for $SrGa_2O_4$: 0.08Eu^{3+}, yBi^{3+} (y = 0.02, 0.05, 0.08, 0.1) phosphors. This decrease in band gap could be the result of co-doping of the Bi^{3+} ion changing the local environment of the lattice. The Bi^{3+} ion produces a certain number of energy levels by forming a continuous band with the $6s^2$ valance electrons. A significant proportion of excited ions may be encouraged to reach higher energy levels due to the decrease in the optical band gap. Therefore, in the presence of Bi^{3+} ions, high emission intensity can be achieved. Bi^{3+} ion concentrations have a significant impact on the optical properties of the phosphors [30].

3.4. Photoluminescence (PL) properties of $SrGa_2O_4$: Eu^{3+}, Bi^{3+} phosphors

3.4.1. Photoluminescence excitation spectra of $SrGa_2O_4$: Eu^{3+}, Bi^{3+} phosphors

Fig. 5 represents the excitation and emission spectrum of $SrGa_2O_4$ phosphor. The excitation band is due to the host absorption and the charge transfer from O^{2-} to Ga^{3+} ions [13,14]. The $SrGa_2O_4$ exhibits self-activated blue emission at 420 nm under the excitation of 225 nm. The presence of Ga^{3+} ions in the octahedral coordinated site serves as the luminescence centre in the host phosphor. Ga^{3+} ions shift from excited energy levels of $^4T_{2B}$, $^4T_1$, $^4T_{2A}$ and ^2E_B to the ground state of $^4A_2$ produce the blue emission [18,19].

Fig. 6 represents the excitation spectra of $SrGa_2O_4$:0.08 Eu^{3+}, yBi^{3+} (y = 0, 0.05) phosphors. A broad band spanning from 250 to 350 nm is caused by the host absorption band overlapping with the CT band of O^{2-} → Eu^{3+} ions, as well as the $^1S_0$ → $^3P_1$ transition of Bi^{3+} ions [5,22,23].

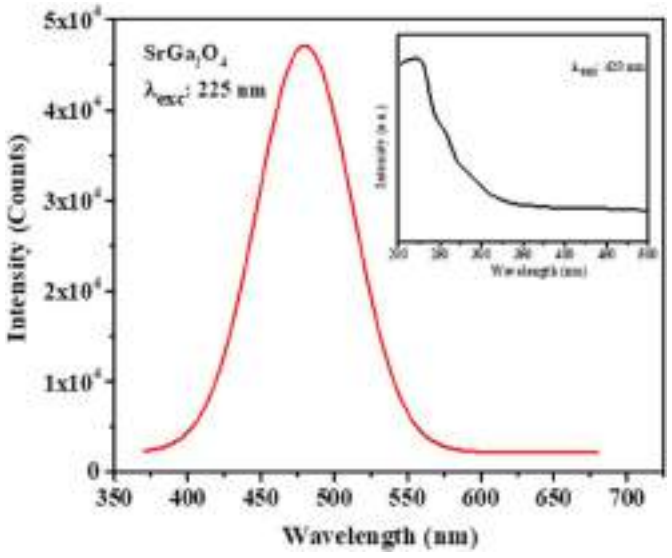

Fig. 5. Emission spectrum of $SrGa_2O_4$ phosphor (inset shows the excitation spectrum of $SrGa_2O_4$ phosphor).

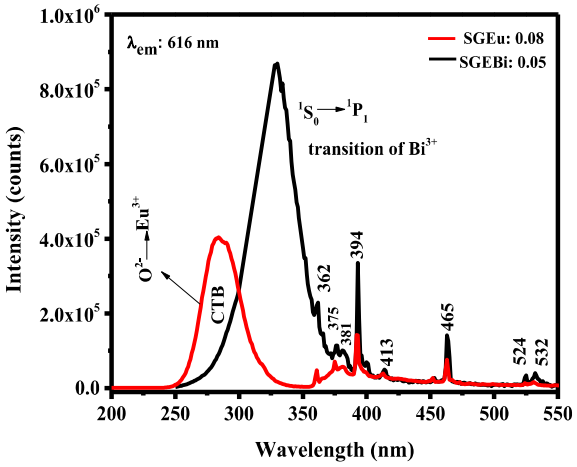

Fig. 6. Excitation spectra of $SrGa_2O_4$: 0.08 Eu^{3+}, yBi^{3+} (y = 0, 0.05) phosphors with emission wavelength at 616 nm.

Bi^{3+} ions typically have a ground state of $^1S_0$ and an outer configuration of $6s^2$. The excited states consist of 6s6p configuration that split into the levels of $^3P_0$, $^3P_1$, $^3P_2$ and $^1P_1$ respectively [20]. The transitions from $^1S_0$ to $^3P_0$ and $^3P_2$ are completely spin forbidden and $^3P_1$ and $^1P_1$ are mixed by spin–orbit coupling. So the emission is starting from $^3P_1$ instead of $^3P_0$ [5–7]. Bi^{3+} ions possess transitions from the ground state $^1S_0$ to $^3P_1$ and $^1P_1$ levels in the excitation spectra. The intensity of CT band significantly increases and get broaden due to the co-doping of Bi^{3+} ions. Its position shifts from 275 to 328 nm from Eu^{3+} doped to Bi^{3+} co-doped phosphors. The broad band centered at 328 nm is due to $^1S_0 \rightarrow {}^3P_1$ transition of Bi^{3+} ions [21]. The excitation peaks assigned at 362, 375, 381, 393, 413, 465, 524 and 532 nm are the characteristic excitation peaks attributed to $^7F_0 \rightarrow {}^5D_4$, $^7F_0 \rightarrow {}^5L_8$, $^7F_0 \rightarrow {}^5L_7$, $^7F_0 \rightarrow {}^5L_6$, $^7F_0 \rightarrow {}^5D_3$, $^7F_0 \rightarrow {}^5D_2$ and $^7F_0 \rightarrow {}^5D_1$ intra-configurational 4f - 4f transitions of Eu^{3+} ions respectively [28–31]. At 382 nm, the edge of the CT band overlaps with the excitation peak of Eu^{3+} ions. In the excitation spectrum, the profile remains the same. It demonstrates that in the NUV region, the broad CT band has higher absorption intensity than that of Eu^{3+} ions in the range of 350–550 nm. Additionally, the significantly higher intensities of the excitation peaks at 465 and 394 nm show that synthesized phosphors can be efficiently excited by blue and near-UV light for the purpose of red light emitting diode applications [33,34]. The energy of the $^3P_1$ level is close to the energy state of $^5L_6$ of Eu^{3+} ion. Generally the emission band of Bi^{3+} ions overlaps with the excitation bands of Eu^{3+} ions. The most favorable regions are mainly at 394 and 465 nm. The energy overlap plays a significant role in energy transfer from sensitizer Bi^{3+} ions to activator Eu^{3+} ions [28]. The energy transfer from the Bi^{3+} to the Eu^{3+} ions can be originate by the electric multipolar and exchange interactions related to the average distance between the Bi^{3+} and Eu^{3+} ions [29].

Fig. 7(a) shows the excitation spectra of $SrGa_2O_4$: 0.08 Eu^{3+}, yBi^{3+} (y = 0, 0.02, 0.05, 0.08, 0.1) phosphors in the range of 200–550 nm under the emission wavelength at 615 nm. The peak shape and excitation peak positions are unaffected by the variations in the Bi^{3+} ions concentration [35–38]. The excitation spectra have similar profile for the Bi^{3+} co-doped and Eu^{3+} doped $SrGa_2O_4$ phosphors [39,40]. The deconvoluted excitation spectrum of $SrGa_2O_4$: 0.08 Eu^{3+}, 0.05Bi^{3+} phosphor is shown in Fig. 7(b).

3.4.2. Photoluminescence emission spectra of $SrGa_2O_4$: Eu^{3+}, Bi^{3+} phosphors

Fig. 8(a) represents the emission spectra of Eu^{3+} doped $SrGa_2O_4$ phosphors excited at 394 nm. The spectra consist of sharp characteristic

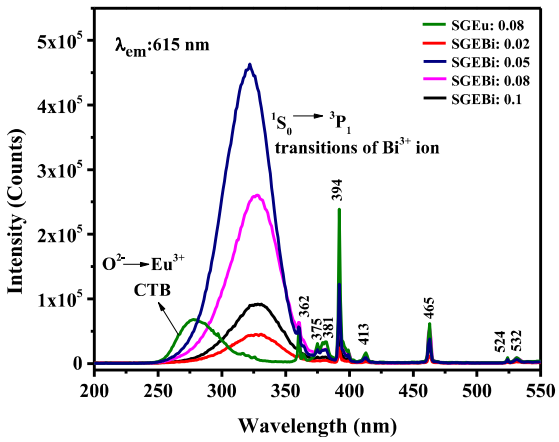

Fig. 7(a). Excitation spectra of Bi^{3+} co-doped $SrGa_2O_4$:0.08 Eu^{3+} phosphors.

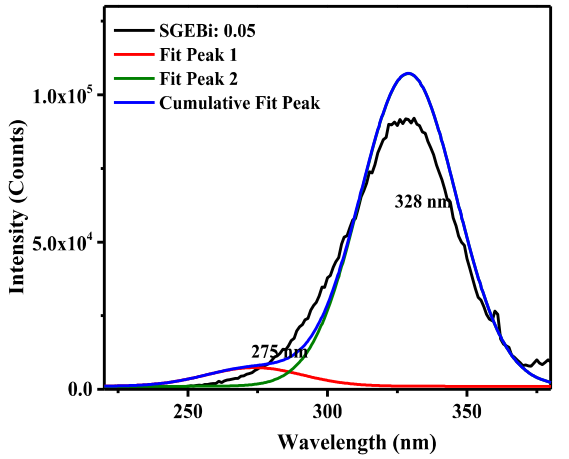

Fig. 7(b). Deconvoluted excitation spectra of $SrGa_2O_4$: 0.08 Eu^{3+}, 0.05Bi^{3+} phosphor.

emission peaks of Eu^{3+} ions in the 550–750 nm range ascribed to the $^5D_0 \rightarrow {}^7F_J$ (J = 0, 1, 2, 3) transitions. The prominent peaks are assigned at 577 ($^5D_0 \rightarrow {}^7F_0$), 587 ($^5D_0 \rightarrow {}^7F_1$), 598 ($^5D_0 \rightarrow {}^7F_1$), 616 ($^5D_0 \rightarrow {}^7F_2$), 645 ($^5D_0 \rightarrow {}^7F_3$) and 654 nm ($^5D_0 \rightarrow {}^7F_3$) respectively [31]. The most intense emission is credited to the hypersensitive forced electric dipole $^5D_0 \rightarrow {}^7F_2$ transition of Eu^{3+} ions at 616 nm. The luminescence emission intensity at 616 nm is stronger than that at 598 nm (magnetic dipole transition), which points out that the Eu^{3+} ion locate at the site without inversion symmetry in the host lattice [32]. The electric dipole (ED) transitions are strongly depends on the local environment of ligands and hence such transitions are hypersensitive in nature [33]. The ED transitions favors when activator ions occupy the site without inversion symmetry and provides red emission for the phosphors. The magnetic dipole transition (MD) transitions are independent of environment of ligand ions and such transitions favors when an activator ion occupies the site with inversion centre. It gives orange red emission for the phosphors [34]. The emission spectra show the same spectral arrangement for different concentrations of Eu^{3+} ions and differ only in their emission intensities. In the present case, ED transition at 616 nm have high emission intensity compared to MD reveals the prominent red emission from the phosphors [35]. The emission at 616 nm increases

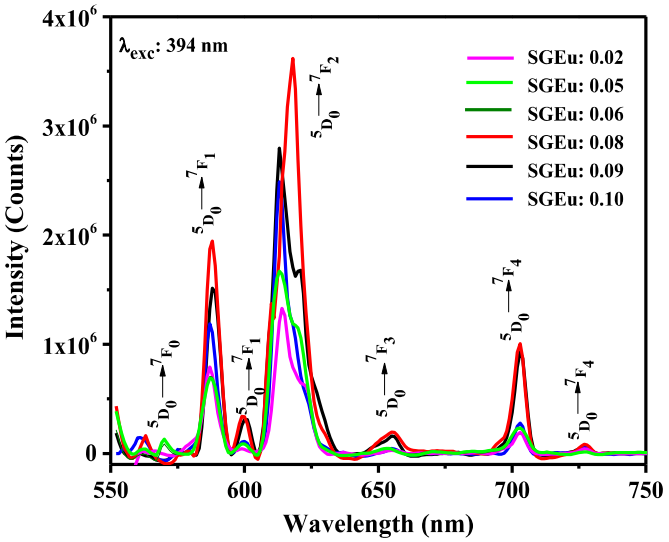

Fig. 8(a). Emission spectra of $Sr_{(1-x)}Ga_2O_4$: xEu^{3+}(x = 0.02, 0.05, 0.06, 0.08, 0.09, 0.1) phosphors excited at 394 nm.

with Eu^{3+} concentration and attains the maximum intensity at x = 0.08 (optimum concentration). Beyond this optimum concentration, quenching of luminescence takes place due to cascade energy transfer among the activator Eu^{3+} ions. The resonant energy transfer becomes stronger and which will enhances the non-radiative relaxation. Thus it causes decrease in emission intensity [37]. Higher dopant concentrations cause the Eu^{3+} ions to move closer to one another by shortening the distance between them and leads to non radiative energy transfer among activator ions. Thus, luminescence intensity decreases for higher doping concentrations. The f-f transitions of Eu^{3+} ions are not significantly affected by the ligands ions because of the shielding effect of the valence electron of the Eu^{3+} ions from 5s and 5p outer electrons [36]. Therefore the emission profile under different concentration of Eu^{3+} ions seems same.

The emission spectra of $Sr_{(1-x-y)}Ga_2O_4$: xEu^{3+}, yBi^{3+} (x = 0.08, y = 0.02, 0.04, 0.05, 0.08, 0.1) phosphors excited at 394 nm is shown in Fig. 8 (b). The emission spectra of Eu^{3+} doped and Bi^{3+} co-doped $SrGa_2O_4$:0.08 Eu^{3+} phosphors have same profile. There is no change in the peak positions of emission lines after the incorporation of Bi^{3+} ions [32]. Emission spectra consists of characteristic emission peaks

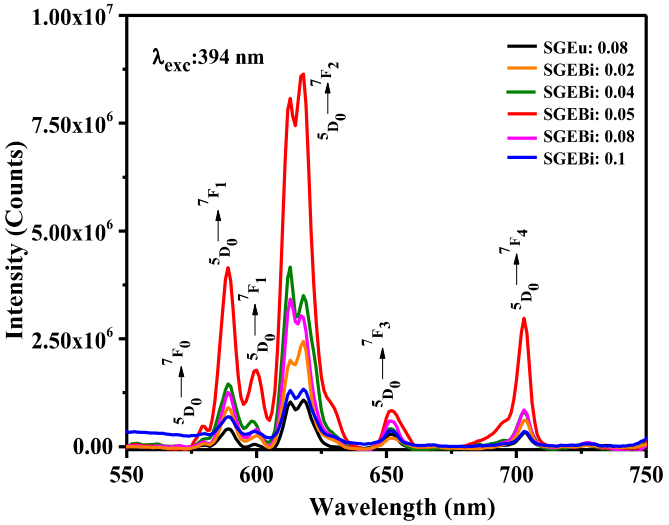

Fig. 8(b). Emission spectra of $Sr_{(1-x-y)}Ga_2O_4$: 0.08Eu^{3+}, yBi^{3+} (y = 0.02, 0.04, 0.05, 0.08, 0.1) phosphors excited at 394 nm.

located at 577 ($^5D_0 \rightarrow ^7F_0$), 587 ($^5D_0 \rightarrow ^7F_1$), 595 ($^5D_0 \rightarrow ^7F_1$), 614, 617 ($^5D_0 \rightarrow ^7F_2$), 652 ($^5D_0 \rightarrow ^7F_3$) and 702 ($^5D_0 \rightarrow ^7F_4$) respectively. The strong red emission ascribed to $^5D_0 \rightarrow ^7F_2$ transitions through forced electric dipole interaction suggests that Eu^{3+} ions are located at the non-inversion symmetry sites within the matrix [35–37]. The spectra also consist of magnetic dipole ($^5D_0 \rightarrow ^7F_1$) interactions of Eu^{3+} ions. The $^5D_0 \rightarrow ^7F_0$ transition indicates that the Eu^{3+} ions are situated in a higher asymmetrical environment [38]. The electric dipole transition is stronger than the magnetic dipole transition indicates the highly asymmetric nature of Eu^{3+} ions and it occupies the site without inversion symmetry in the host lattice [39]. Bi^{3+} concentration enhances the emission intensity of Eu^{3+} ions up to y = 0.05. Emission intensity decreases beyond this concentration level due to the sensitization effect of Bi^{3+} on Eu^{3+} ions [40]. In the presence of Bi^{3+} ions, the intensity of red emission increases significantly compared to that of Eu^{3+} doped $SrGa_2O_4$ phosphor [41–43]. Because of the difference in ionic radius between Bi^{3+} and Eu^{3+} ions, co-doping of bismuth ions modifies the crystal field surrounding the Eu^{3+} ion. Bi^{3+} ions have a slightly larger ionic radius than Eu^{3+} ions. Here, the ionic radius of the dopant ion is smaller than that of the sensitizer ion. It causes more lattice deformation and may intensify the red emission [44]. The light absorbed by the sensitizer Bi^{3+} ions transferred to the activator Eu^{3+} ions. Consequently, it enhances the emission of Eu^{3+} ions in the $SrGa_2O_4$ host by efficiently transferring energy from Bi^{3+} to Eu^{3+} ions [45]. Further increase in the concentrations of Bi^{3+} ions blocks the luminescence intensity. Therefore, the extent to which the red emission of Eu^{3+} ions is enhanced depends on the most favorable energy transfer from sensitizer Bi ions to activator Eu^{3+} ions [41]. Higher concentrations of Bi^{3+} ions have the potential to cause ion aggregation, which can function as trapping sites within the host lattice. Bi^{3+} ions non-radiatively transfer the received energy results in the reduction of luminescence intensity of Eu^{3+} ions [42,43].

The asymmetric ratio is significant for predicting the local symmetry of Eu^{3+} ions and gives information about the asymmetric nature in the neighborhood of Eu^{3+} ions. It can be calculated by the ratio of the integral intensity of the electric dipole transition ($^5D_0 \rightarrow ^7F_2$) to magnetic dipole transition ($^5D_0 \rightarrow ^7F_1$) of Eu^{3+} ions. In the present study, the red emission attributed to electric dipole transition (ED) transition at 616 nm is more prominent than magnetic dipole transition (MD) transitions [46]. This can be further confirmed from the asymmetric ratio values. If the asymmetry ratio values are less than 1, which demonstrates the predominance of the magnetic dipole $^5D_0 \rightarrow ^7F_1$ transition whereas the value is greater than 1, then it shows the predominance of electric dipole $^5D_0 \rightarrow ^7F_2$ transitions of Eu^{3+} ions in host lattice [38,47]. From the emission spectra, the R values for various concentrations of Bi^{3+} ions are greater than 1 indicates that the electric dipole transition dominates over other transitions [48]. Fig. 9 depicts the energy level diagram between the sensitizer Bi^{3+} ions and the Eu^{3+} ions.

Fig. 10 represents the emission spectra of $Sr_{(1-x-y)}Ga_2O_4$: $0.08Eu^{3+}$, yBi^{3+} (y = 0.02, 0.05, 0.08, 0.1) phosphors excited at 360 nm. The broad bluish-green emission band ranges from 400 to 550 nm centered at 465 nm is originated by the transition of electrons from the excited states of the Bi^{3+} ions to ground state corresponds to $^3P_1 \rightarrow ^1S_0$ transitions [43]. The red emission lines of Eu^{3+} ions are recorded in the range of 570–720 nm confirms the incorporation of both Bi^{3+} and Eu^{3+} ions into the host $SrGa_2O_4$ phosphor. The characteristic emission of Eu^{3+} ions assigned at 575, 589, 592, 615, 617, 653 and 686 nm ascribed to $^5D_0 \rightarrow ^7F_{0\text{-}4}$ transitions respectively [48,49]. The transfer of electrons to higher excited states of Eu^{3+} ions radiatively comes back to ground state through $^5D_0 \rightarrow ^7F_j$ transitions results in the red emissions [38]. The intensity of the broad emission increases with concentration of Bi^{3+} ions. In this luminescence process, energy will be transferred from host to Bi^{3+} ions and subsequently absorbed by the activator Eu^{3+} ions [23–25]. No change is observed in the broad emission band or the peak positions of Eu^{3+} ions.

3.4.3. *The excitation and emission spectra of $SrGa_2O_4$: Bi^{3+} phosphor*

Fig. 11(a) shows the photoluminescence excitation spectra of the Bi^{3+} doped $SrGa_2O_4$ phosphor monitored at emission wavelength of 495 nm respectively. The excitation peak recorded at 330 nm is attributed to $^1S_0 \rightarrow ^3P_1$ transitions of Bi^{3+} ions [50].

The corresponding emission spectrum of $SrGa_2O_4$: $0.05Bi^{3+}$ phosphor excited at 330 nm is shown in Fig. 11(b). The broad bluish green emission band in the range 350–650 nm centered at 495 nm is attributed to $^3P_1 \rightarrow ^1S_0$ transition of Bi^{3+} ions. Wang et al. (2017) reported the broad emission band of $CaGa_2O_4$: Bi^{3+} phosphor in the range of 400–700 nm [50]. The ground state of Bi^{3+} ion is $^1S_0$ and the excited states are $^3P_{0,1,2}$ and $^1P_1$ respectively. The electrons in the ground state $^1S_0$ of Bi^{3+} ions absorb energy and make transition to the $^3P_1$ energy state [51,52].

The energy overlap plays a significant role in energy transfer from sensitizer Bi^{3+} ions to activator Eu^{3+} ions and it is shown in Fig. 11(c). It is known that the emission band of Bi^{3+} in the range of 300–600 nm overlap with the partial excitation peaks of Eu^{3+} ions [45–47]. The ground state of Bi^{3+} ion is $^1S_0$ and its excited states gives $^3P_0$, $^3P_1$, $^3P_2$ triplet and $^1p_1$ singlet levels [11–15]. Bi^{3+} ions excited with UV light, there is an electronic transition from $^1S_0$ to $^3P_1$ and $^1P_1$ levels. The transition to $^3P_0$ and $^3P_2$ are generally forbidden. Therefore $^1S_0 \rightarrow ^3P_1$ and $^1S_0 \rightarrow ^1P_1$ transitions produce emission from the Bi^{3+} ions. There is a spectral overlap between excitation spectrum of Eu^{3+} ions with emission

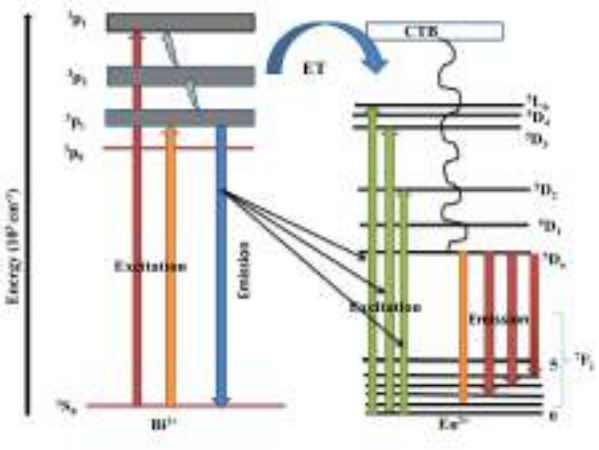

Fig. 9. The energy level diagram between sensitizer Bi^{3+} ions to Eu^{3+} ions in $SrGa_2O_4$: Eu^{3+}, Bi^{3+} phosphors.

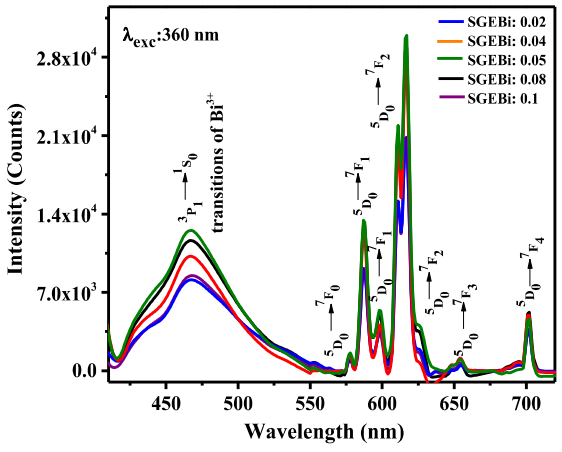

Fig. 10. Emission spectra of $Sr_{(1-x-y)}Ga_2O_4$: xEu^{3+}, yBi^{3+} (x = 0.08, y = 0.02, 0.05, 0.08, 0.1) phosphors excited at 360 nm.

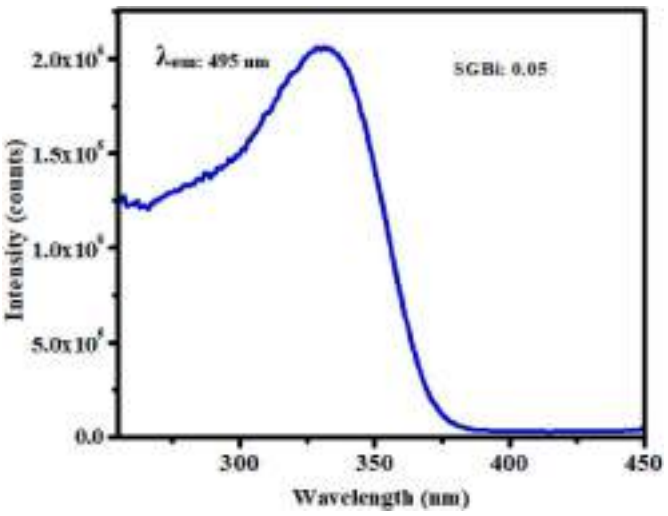

Fig. 11(a). Excitation spectrum of Bi^{3+} doped $SrGa_2O_4$ phosphor.

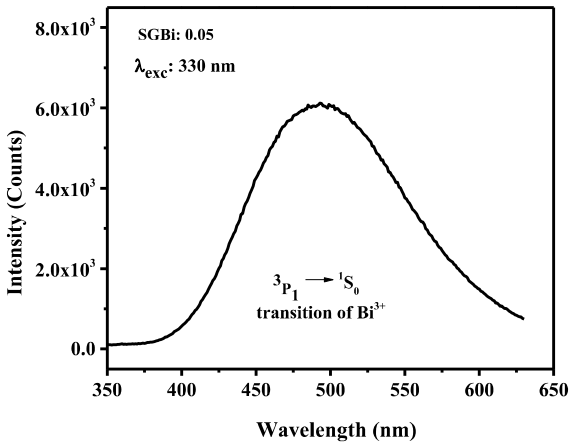

Fig. 11(b). Emission spectrum of Bi^{3+} doped $SrGa_2O_4$ phosphors.

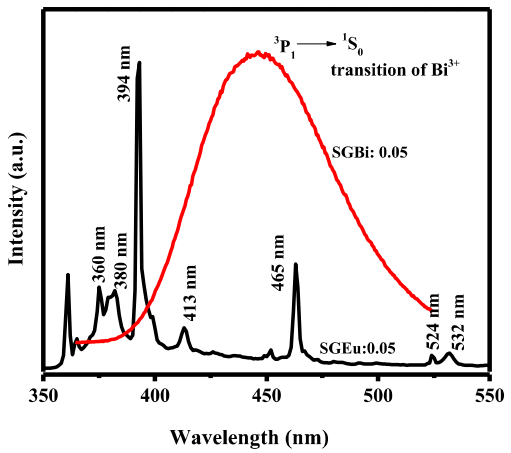

Fig. 11(c). Overlapping of emission band of Bi^{3+} ions with excitation peaks of Eu^{3+} ions.

band of Bi^{3+} ions in the host $SrGa_2O_4$ phosphor and it favors effective energy transfer from Bi^{3+}→ Eu^{3+} ions. The broad luminescence emission band is originate from the transitions of some of the electrons in the excited states comes back to the ground state by radiative transitions. The remaining electrons present in the bismuth ions transfer its energy to the activator Eu^{3+} ions and produce red emission lines [12]. Electrons in the ground state of the Eu^{3+} ions are stimulated to the $^5L_6$ and $^5D_3$ levels after receiving energy from the Bi^{3+} ions. After a specific duration, electrons stay in that state and then radiatively relax to the $^5D_0$ state, producing distinct emission lines of europium ions that are attributed to the $^5D_0 \rightarrow {}^7F_j$ (j = 0, 1, 2, 3, 4) transitions. It proves the significant energy transfer from sensitizer Bi^{3+} ions to activator Eu^{3+} ions. The $^3P_1$ energy state of Bi^{3+} ion is close to that of $^5L_6$ energy level of Eu^{3+} ion. The electrons present in the $^5L_6$ state relax to the first excited $^5D_0$ state without radiation, and then comes back to the ground ^7F_J (J = 0, 1, 2, 3, 4) state results in the enhanced red emission [15]. It favors the $^5D_0 \rightarrow {}^7F_2$ transitions of Eu^{3+} ions. Such overlapping further confirmed the effective energy transfer between Bi^{3+}→Eu^{3+} ions. Hekai Zhu et al. (2013) reported the similar overlapping of emission band of Bi^{3+} ions and excitation bands of Eu^{3+} ions in Bi^{3+}/Eu^{3+} co-doped $Ca_{10}(PO_4)_6F_2$ phosphors [53].

3.4.4. Color characteristics

The performance of synthesized phosphors can be analyzed from the Commission Internationale de l'Eclairage (CIE) chromaticity diagram. CIE coordinates are very helpful for the prediction of colors exhibited by the phosphors. Purity of the observed color from a phosphor is decided by the CIE coordinates, which can be calculated from the emission spectrum [18]. The CIE chromaticity diagram of $Sr_{(1-x-y)}Ga_2O_4$:$0.08Eu^{3+}$, yBi^{3+} (y = 0.02, 0.04, 0.05, 0.08, 0.1) phosphors under the excitation at 394 nm is shown in Fig. 12. The chromaticity coordinates are calculated to be (0.610, 0.381), (0.646, 0.346), (0.650, 0.343), (0.658, 0.337), (0.640, 0.350) and (0.636, 0.352) for y = 0, 0.02, 0.04, 0.05, 0.08 and 0.1 respectively. These color coordinates are closer to standard NTSC value of red emission (x = 0.67, y = 0.33) [30]. The color coordinates enhances from (0.610, 0.381) of Eu^{3+} doped phosphor to (0.658, 0.337) that of Bi^{3+} co-doped phosphor. CIE diagram demonstrates the effect of Bi^{3+} co-doping on the enhancement of red emission in Eu^{3+} ions due to the energy transfer from Bi^{3+} ions to Eu^{3+} ions. The obtained CIE values are better than commercial Y_2O_3:Eu^{3+} red

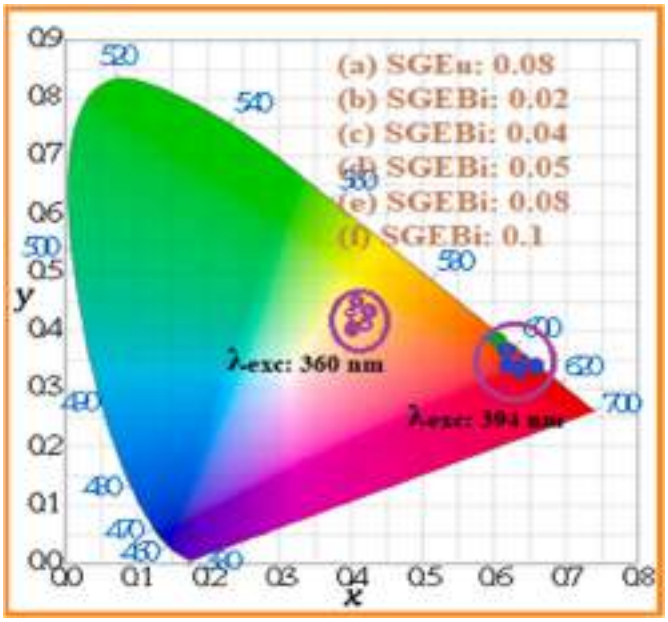

Fig. 12. CIE diagram of $Sr_{(1-x-y)}Ga_2O_4$: xEu^{3+}, yBi^{3+} (x = 0.08, y = 0.02, 0.05, 0.08, 0.1) phosphors excited at 394 and 360 nm.

phosphor (0.64, 0.36). It indicates the potential applications of these phosphors in the field of UV or NUV- LEDs and WLEDs [54,55].

Color purity (CP) is very important factor for the suitability of a phosphor in the display as well as light emitting device applications [56]. The color purity can be calculated with the help of CIE coordinates using the equation

$$CP = \frac{\sqrt{(X_s - X_i)^2 + (Y_s - Y_i)^2}}{\sqrt{(X_d - X_i)^2 + (Y_d - Y_i)^2}} * 100 \quad (2)$$

here (x_s, y_s), (x_i, y_i), (x_d, y_d) denotes the coordinates of a sample point, equal energy point (0.333, 0.333) of illuminant and coordinates of the dominant wavelength respectively [41]. The color purity of $SrGa_2O_4$: $0.08Eu^{3+}$ phosphor is obtained as 97.4 %. The color purity of the phosphors increases with Bi^{3+} co-doping. The maximum color purity is calculated to be 98.6 % for $SrGa_2O_4$: $0.08Eu^{3+}$, $0.05\ Bi^{3+}$ phosphor. It shows the high quality red-emitting property of Bi^{3+} co-doped $SrGa_2O_4$: $0.08Eu^{3+}$ phosphors [57].

Correlated color temperature (CCT) is another important parameter to verify theefficiency of phosphor and which specifies the color temperature of light emitted from the phosphors in degrees Kelvin (K) [50]. CCT rating is a general indicator of the warmth or coolness of a source. The CCT values can be determined using McCamy empirical equation

$$CCT = -449n^3 + 3525n^2 - 6823.3n + 5520.33 \quad (3)$$

here n represents $(x-x_e)/(y-y_e)$ and the chromaticity epicenter is located at $x_e = 0.332$, $y_e = 0.186$. It is well known that CCT values below 3200 K are generally treated as warm light sources, while those with value greater than 4000 K are normally cool in appearance. For domestic lighting applications, the preferred CCT value is below 3200 K. In this study, the CCT values below 2000K suggest that the prepared phosphors can be effectively used in the fabrication of warm LEDs applications [41,42]. The CIE coordinates, color purity and correlated color temperature of $Sr_{(1-x-y)}Ga_2O_4$:x Eu^{3+}, yBi^{3+}(x = 0.08, y = 0.02, 0.04, 0.05, 0.08, 0.1) phosphors are tabulated in Table 2.

The CIE coordinates of $Sr_{(1-x-y)}Ga_2O_4$: xEu^{3+}, yBi^{3+} (x = 0.08, y = 0.02, 0.05, 0.08, 0.1) phosphors excited at 360 nm is shown in Fig. 12. The color co-ordinates lie in the yellow orange region of the chromaticity diagram. It demonstrates that tunable emission is possible by choosing the right excitation wavelength because Bi^{3+} ions can exhibit a wide range of emission colors [40,58]. These phosphors can be used in phosphor-converted UV-LEDs due to their tunable emission properties. The CIE and CCT for different concentration of Bi^{3+} in $SrGa_2O_4$: $0.08Eu^{3+}$ phosphors are summarized in Table 3.

3.5. Life time analysis

Figs. 13 and 14(a-d) depict the kinetic decay curves for the emission of $SrGa_2O4$: 0.08 Eu^{3+} and $SrGa_2O_4$:0.08 Eu^{3+}, yBi^{3+} (y = 0, 0.02, 0.05, 0.08, 0.1) phosphors excited at 394 nm. The luminescence decay curve can be fitted with the exponential function. The decay time

Table 2
The CIE coordinates, color purity and correlated color temperature of $Sr_{(1-x-y)}Ga_2O_4$: xEu^{3+}, yBi^{3+} (x = 0.08, y = 0.02, 0.05, 0.08, 0.1) phosphors excited at 394 nm.

Sample code	Excitation 394 nm	CCT (K)	Color purity (%)
	CIE coordinates (x, y)		
SGEu: 0.08	(0.6101, 0.3810)	1324	97.40
SGEBi:0.02	(0.6462, 0.3462)	1030	97.70
SGEBi:0.04	(0.6501, 0.3431)	1004	98.02
SGEBi:0.05	(0.6582, 0.3370)	1000	98.60
SGEBi:0.08	(0.6400, 0.3503)	1069	97.13
SGEBi:0.1	(0.6362, 0.3521)	1092	96.50

Table 3
The CIE coordinates and correlated color temperature of $Sr_{(1-x-y)}Ga_2O_4$:xEu^{3+}, yBi^{3+} (x = 0.08, y = 0.02, 0.05, 0.08, 0.1) phosphors excited at 360 nm.

Phosphor	Excitation = 360 nm	CCT (K)
	CIE coordinates (x, y)	
SGEBi:0.02	(0.401, 0.436)	2887
SGEBi: 0.04	(0407, 0.439)	2893
SGEBi:0.05	(0.420, 0.417)	2556
SGEBi:0.08	(0.416, 0.428)	2647
SGEBi:0.1	(0.408, 0.435)	2726

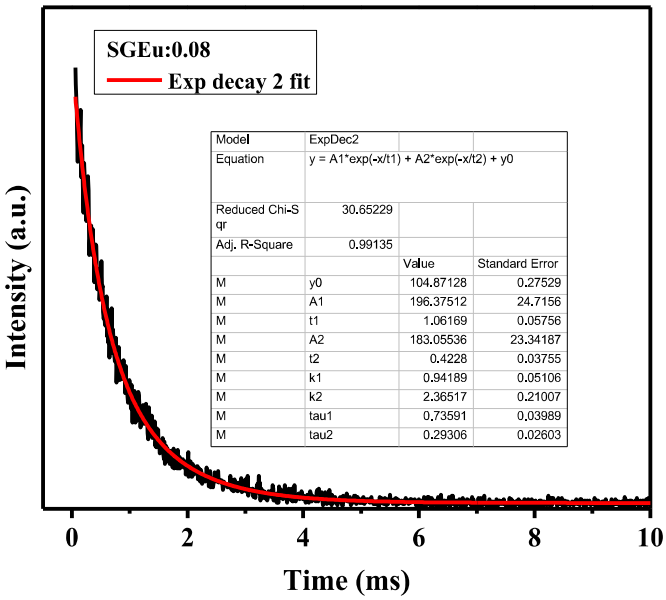

Fig. 13. Lifetime measurement of $SrGa_2O_4$: $0.08Eu^{3+}$ phosphor.

corresponding to the particular excitation was calculated using the principle of the exponential formula given in equation (4).

$$I = A_1 \exp(-t/\tau_1) + A_2 \exp(-t/\tau_2) \quad (4)$$

where, I is phosphorescence intensity, A_1, A_2 are constants, t is time, τ_1 and τ_2 are decay times for the exponential components. Initially intensity undergo very fast decaying and further decaying takes place very slowly [35,36]. From the graph the value of $\tau_1 = 0.735$ ms and $\tau_2 = 0.293$ ms for Eu^{3+} doped phosphor. After the co-doping of Bi ions, the lifetime values decreases [31]. The life time values of $SrGa_2O_4$:0.08 Eu^{3+}, yBi^{3+} (y = 0.02, 0.05, 0.08, 0.1) phosphors are found to be $\tau_1 = 0.325$ ms, $\tau_2 = 0.046$ ms, $\tau_1 = 0.242$ ms, $\tau_2 = 0.022$ ms, $\tau_1 = 0.238$ ms, $\tau_2 = 0.0311$ ms, $\tau_1 = 0.228$ ms, $\tau_2 = 0.023$ ms respectively. It further confirms the effective energy transfer from Bi^{3+} to Eu^{3+} ions. The incorporation of Bi^{3+} ions can enhance luminescent intensity of Eu^{3+} ions by means of reducing the decay time of excited electrons in $^5D_0$ level of Eu^{3+} ions [38].

3.6. Quantum efficiency (QE)

Quantum efficiency is one of the crucial criteria used to determine a phosphor's appropriateness for usage in white LED devices. The QE of the $SrGa_2O_4$: $0.08Eu^{3+}$, $0.05Bi^{3+}$ phosphors excited at 394 nm is calculated using the following equation

$$QE = \frac{\int L_S}{\int E_R - \int E_S} \quad (5)$$

where L_S is the emission spectrum of the phosphor, E_S and E_R represents

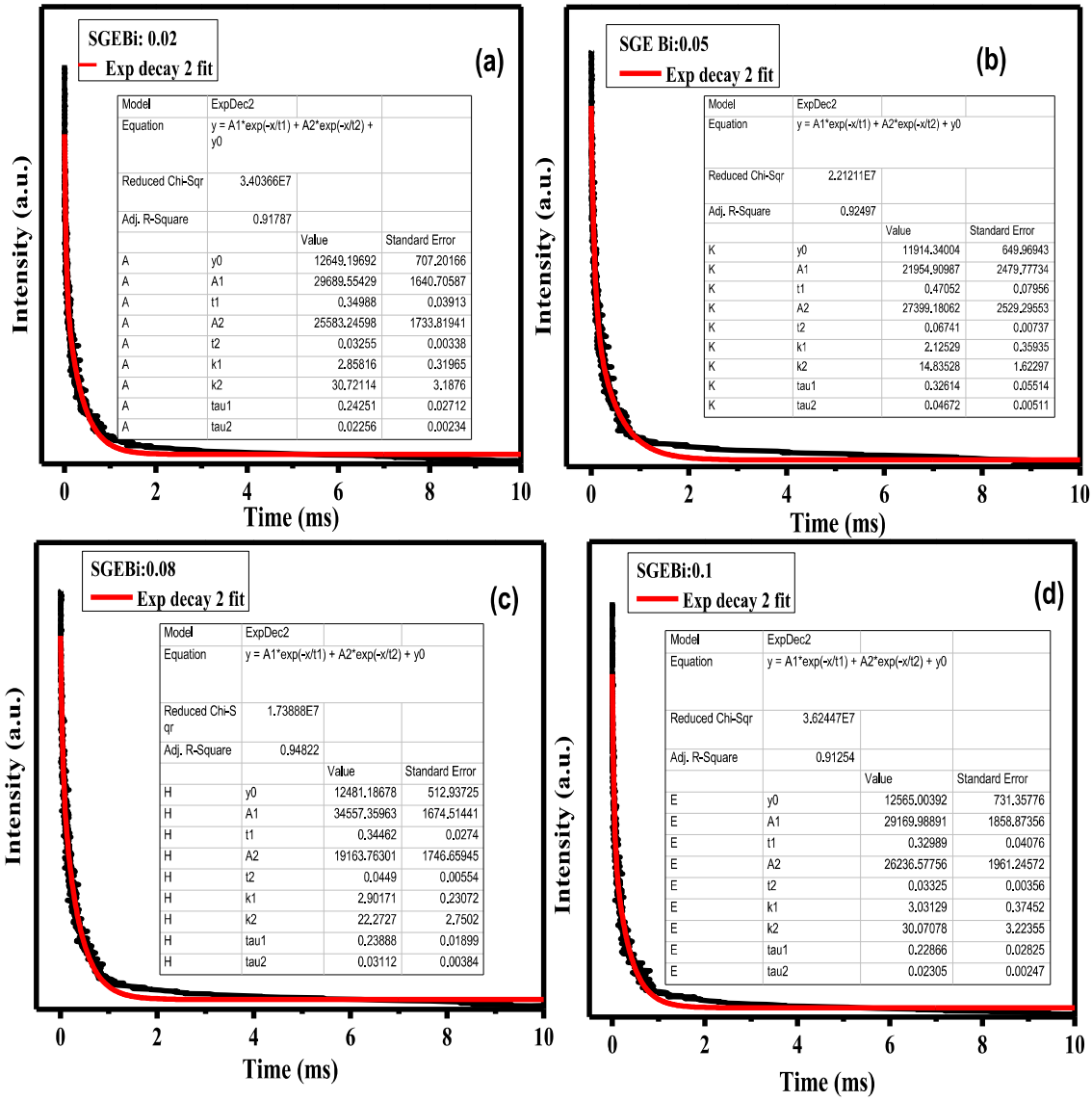

Fig. 14. (a–d) Lifetime measurement of $Sr_{(1-x-y)}Ga_2O_4$:0.08Eu^{3+}, yBi^{3+} (y = 0.02, 0.05, 0.08, 0.1) phosphors excited at 394 nm.

the excitation spectra with and without the phosphor respectively [39]. Based on the recorded emission spectra, the QE of $SrGa_2O_4$: 0.08Eu^{3+}, yBi^{3+} (y = 0.02, 0.05, 0.08, 0.1) phosphors are found to be 9.21, 12.42, 11.56 and 7.23 % respectively. The comparatively good quantum efficiency reveals the UV- driven WLED application of these synthesized phosphors.

3.7. Temperature dependent photoluminescence (TDPL)

Thermal stability is one of the most essential factors to take into account when analyzing the effectiveness of phosphors in WLEDs. Fig. 15 (a) displays the temperature dependent photoluminescence spectra of $SrGa_2O_4$: 0.08 Eu^{3+}, 0.05 Bi^{3+} phosphor excited at 394 nm, which is obtained by recording temperature increases from ambient temperature 298 K–483 K at intervals of 20 K. For different temperatures, the spectra show the same emission profiles. The emission intensity decreases as the temperature increases from ambient to 483 K [32]. In general, the thermal quenching occurs when the photoluminescence intensity reduces to 50% of its initial value at 423 K [43,44]. Even though the emission intensity gradually decreases with increasing temperature, at 423 K it still retains 96.7% of the initial value (298 K). In the present study, there is no such quenching observed, the optimized phosphor exhibits excellent thermal stability at elevated temperatures.

To evaluate the thermal stability of luminous materials, it is necessary to calculate the activation energy (ΔE) of thermal quenching. As ΔE increases, the phosphor gains thermal stability. The Arrhenius plot is used to calculate the activation energy ΔE. The relationship between the temperature and the intensity of phosphor emission is connected by the Arrhenius activation model. Arrhenius equation is given below.

$$I_{(T)} = \frac{I_0}{1 + cexp\left(-\frac{\Delta E}{kT}\right)} \quad (6)$$

here I_0 is the emission intensity at initial temperature, $I_{(T)}$ denotes intensity at temperature T, c constant, k is the Boltzmann's constant and its value $8.62*10^{-5}$ eVK^{-1} [45]. From the Arrhenius equation, the graph of ln [(I_0/I_T) −1] versus 1/kT is shown in Fig. 15(b). The slope of the straight line is −0.253 and it gives the value of activation energyΔE to be 0.253 eV. This relatively high activation energy confirms the better

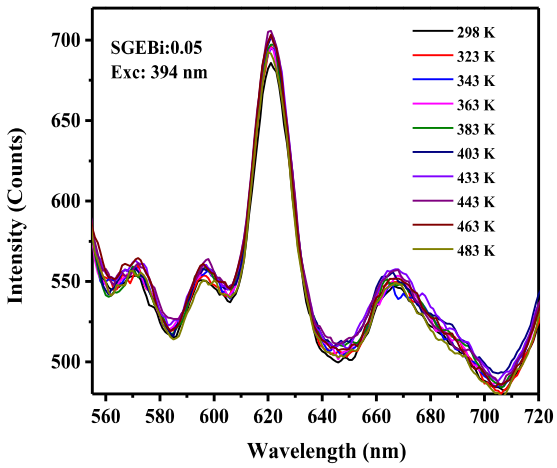

Fig. 15(a). The temperature dependent emission spectra of $SrGa_2O_4$: 0.08 Eu^{3+}, 0.05 Bi^{3+} phosphor excited by 394 nm recorded from 298 to 483 K.

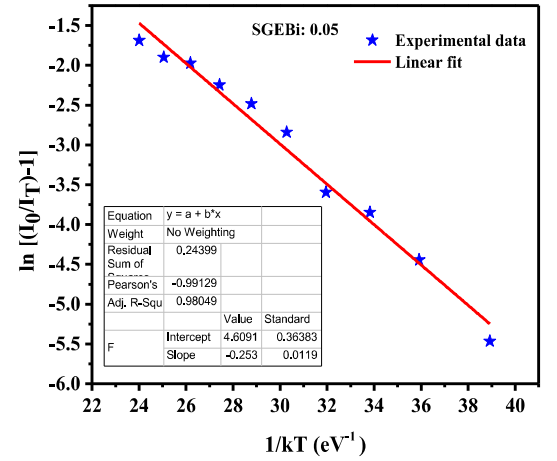

Fig. 15(b). The Arrhenius plot of temperature dependence on the PL emission intensity of $SrGa_2O_4$: 0.08 Eu^{3+}, 0.05 Bi^{3+} phosphor.

thermal stability of the phosphor. It further supports the future applications of the synthesized phosphors as acceptable red emitters in solid state lighting and WLEDs technologies [46,47].

3.8. Mechanoluminescence studies (ML)

The mechanoluminescence properties of synthesized phosphors are measured by dropping a load of mass 100 g is dropped from different heights. The ML glow curve of undoped and $SrGa_2O_4$: 0.08Eu^{3+}, yBi^{3+} (y = 0, 0.02, 0.04, 0.05, 0.08, 0.1) phosphors at a height of 25 cm is shown in Fig. 16(a). The undoped and Eu^{3+} doped $SrGa_2O_4$ phosphors show intense single emission peak as a function of ML intensity versus time in the ML glow curve [14]. The narrow single peak in the ML glow curve is attributed to some charge transfer process involved during the process [59]. It quickly induces a number of physical and chemical responses inside the phosphor. The deformation that mechanical force creates on the phosphor's surface is the primary cause of ML emission [16,18]. The phosphor emits light in response to a mechanical stimulation as a result of the recombination of holes at the luminescence

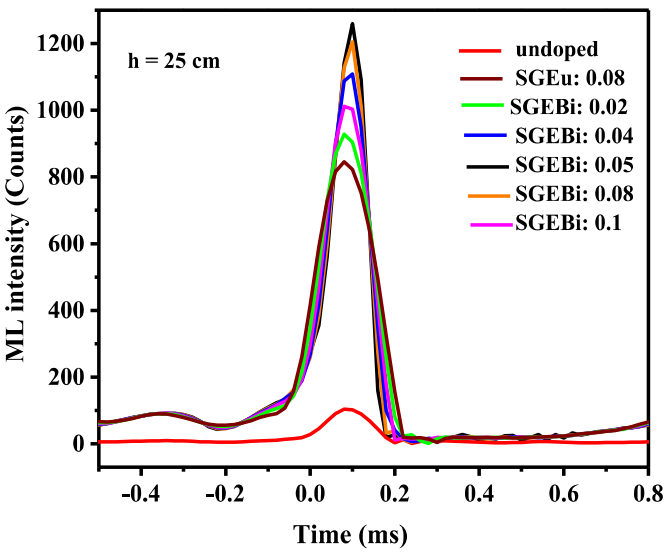

Fig. 16 (a). Mechanoluminescence signal intensity with time of $Sr_{(1-x-y)}Ga_2O_4$: xEu^{3+}, yBi^{3+} (x = 0.08, y = 0.02, 0.04, 0.05, 0.08, 0.1) phosphors.

centre with electrons in the conduction band [60]. The intensity of the ML peak is further increased by the co-dopant Bi^{3+} ions without changing the position or the shape of the glow curve. During testing, ML materials have to be brought into contact with different kinds of materials such as glass or metals generate mechanical stimulations. Such mechanical stimulation causes the internal fractures in the material and produce newly formed surfaces. These fracture or deformation create charge separation and a strong electric field about 10^7 - 10^8 Vm^{-1} develop on the newly formed surfaces. Thus, electrons in the conduction band have two possible outcomes: they can either recombine immediately with the holes in the luminescence or recombination centres, or they can spend some time in the trapped centres close to the conduction band [7]. These charges subsequently combine to generate excitons further initiate emission processes [61].

The variation of ML intensity with Bi^{3+} concentration is depicted in Fig. 16(b). The influence of dopant concentration on the intensity of the ML glow curve is consistent with the outcome of PL emission [37]. The ML intensity in the glow curve increases as the concentration of Bi^{3+} ions rises, reaching a maximum intensity at y = 0.05, after which the

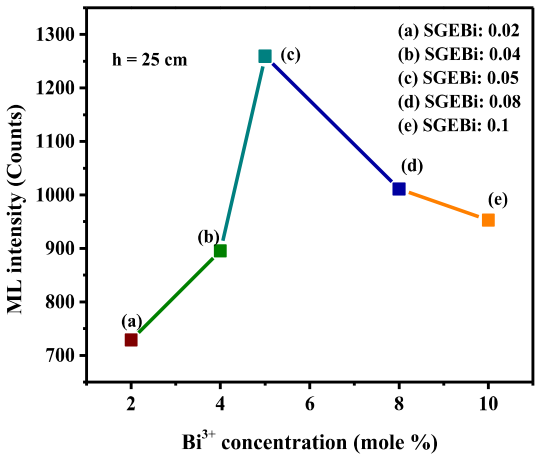

Fig. 16(b). Variation in ML intensity with different Bi^{3+} concentrations in $SrGa_2O_4$:0.08Eu^{3+} phosphors.

luminescence begins to quench. The decrease in the distance between free charge carriers may be the cause of the decrease in ML intensity at higher dopant concentrations. A reduction in luminescence intensity results from the ease of energy transfer between free charge carriers [62]. Maximum emission is obtained for $SrGa_2O_4$: $0.08Eu^{3+}$, $0.05Bi^{3+}$ phosphor.

Fig. 16(c) represents variation in the intensity of ML glow curve for different dropping heights of the load [14]. ML intensity is proportional to the impact height and square of the impact velocity. When the impact height increases, more area is provided for fractured charged surfaces and it further results in the enhancement of recombination luminescence [14,15]. The maximum ML intensity is attained for a height 25 cm.

The change in ML intensity with impact velocity is depicts in Fig. 16 (d). The impact velocity can be determined using the equation $(2gh)^{1/2}$ where g is acceleration due to gravity and h is the falling height [50]. As the velocity of the piston increases with height, the impact velocity will be more and hence more fractures are created in the sample which results in the creation of new surface [15–17]. ML intensity increases linearly with impact velocity. The increase in impact velocity increases the piezoelectricity and it provides the chance for more number of electrons to get ionized and reach the conduction band [61,62]. More electrons will therefore reach the centres for luminescence or recombination to recombine with the pre-existing holes [63,64]. These may be the possible reasons behind the peak ML intensity increasing with impact velocity [65]. These studies show that as synthesized phosphors can serve as a component in stress sensor applications [65].

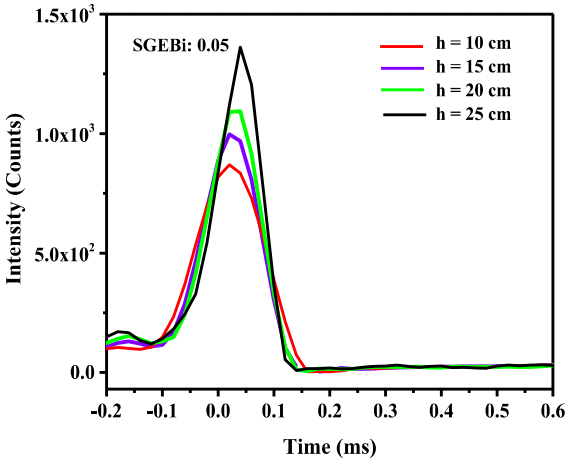

Fig. 16(c). Variation in ML intensity with different dropping heights in $SrGa_2O_4$:$0.08Eu^{3+}$, $0.05Bi^{3+}$ phosphors.

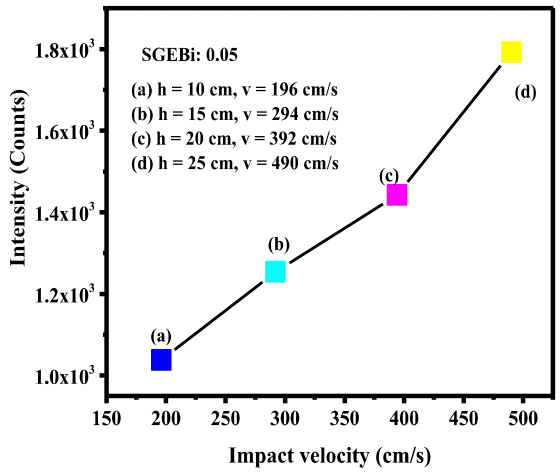

Fig. 16 (d). Impact velocity dependence on total ML intensity of $SrGa_2O_4$:$0.08Eu^{3+}$, $0.05Bi^{3+}$ phosphors.

4. Conclusions

The Bi^{3+} co-doped red emitting $SrGa_2O_4$:$0.08Eu^{3+}$ phosphors have been successfully synthesized by solid state reaction method. The synthesized phosphors exist in single phase with monoclinic structure. The doping of Eu^{3+} and co-doping of Bi^{3+} ions does not change the crystal structure as well as phase of the host matrix. Eu^{3+} doped and Bi^{3+} co-doped $SrGa_2O_4$ phosphors exhibit sharp intense red emission attributed to hypersensitive electric dipole ($^5D_0 \rightarrow {}^7F_2$) transition at 615 nm and it indicates the occupation of Eu^{3+} ions in the site lack of inversion symmetry in the lattice. The presence of Bi^{3+} ions significantly enhances the red emission of Eu^{3+} ions due to the effective energy transfer between Bi^{3+} and Eu^{3+} ions. The emission band of Bi^{3+} ions partially overlapped with excitation peaks of Eu^{3+} ions especially in the region 380–500 nm. Such overlapping provides the better energy transfer mechanism between the sensitizer and activator ions. The emission spectra excited at 360 nm shows the bluish white emission. By varying the excitation wavelength, tunability of colour emission can be achieved from the synthesized phosphors. The color purity increases from 97.4 to 98.6 % after the co-doping of Bi^{3+} ions. The optimized $SrGa_2O_4$: 0.08 Eu^{3+}, 0.05 Bi^{3+} phosphor exhibits high thermal stability of 96.7% with activation energy of 0.253 eV. It indicates the possibility of this phosphor in LEDs operating in hot environments. A single peak is obtained in the ML glow curve without any irradiation for undoped, Eu^{3+} doped as well as Bi^{3+} co-doped phosphors. The intensity of ML glow curve enhanced after the incorporation of Bi^{3+} ions due to the formation of newly developed defects produced in the phosphor surface. The ML intensity increased from y = 1–5 mol % then decreases with the doping concentration of Bi^{3+} ions. This result is consistent with the PL emission. The ML intensity increases with impact velocity. The luminescence studies suggest that the synthesized phosphors can be used as suitable red emitter in phosphor converted WLEDs, solid state light emitting diodes, sensors and stress indicators etc.

CRediT authorship contribution statement

B. Vasanthi: Writing – review & editing, Writing – original draft, Visualization, Software, Resources, Methodology, Investigation, Formal analysis, Data curation, Conceptualization. **N. Gopakumar:** Writing – review & editing, Visualization, Validation, Supervision, Conceptualization. **P.S. Anjana:** Writing – review & editing, Validation, Supervision, Conceptualization.

Declaration of competing interest

The authors declare that they have no known competing financial interests or personal relationships that could have appeared to influence the work reported in this paper.

Data availability

The data that has been used is confidential.

Acknowledgement

The authors are thankful to the Department of Physics, University of Kerala, Kariavattom Campus for X-ray diffraction analysis measurements. The authors are grateful to Department of Optoelectronics,

University of Kerala, Kariavattom Campus for FESEM, UV–Visible studies. The authors are grateful to CLIF, University of Kerala, Trivandrum for EDAX, PL and lifetime analysis. The authors are thankful to SAIF, MG University for PL analysis. The authors are thankful to SSN College of Engineering, Kalavakkam for TDPL analysis.

References

[1] F.P. Glasser, L.S. Dent Glasser, Crystal chemistry of some AB_2O_4, compounds, J. Am. Ceram. Soc. 46 (8) (2006) 377–380, https://doi.org/10.1111/j.1151-2916.1963.tb11755.x.

[2] Mohamed Bououdin Al-Najar, Mamdouh Abdel Aal Ahmed, Catalytic and Tetiana Tatarchuk, Basma, Photocatalytic Properties of Oxide Spinels, 2018, pp. 1–50, https://doi.org/10.1007/978-3-319-48281-1_158-1, hand book of ecomaterials.

[3] Volker Kahlenberg, Claudia Weidenthaler, High temperature single crystal diffraction study on monobarium gallate - the crystal structure of β-$Baga_2O_4$, Solid State Sci. 4 (2002) 963–968, https://doi.org/10.1016/S1293-2558(02)01351-1.

[4] Volker Kahlenberg, Valerie Goettgens, Philipp Mair, Daniela Schmidmair, High-pressure synthesis and crystal structures of the strontium oxogallates $Sr_2Ga_2O_5$ and $Sr_5Ga_6O_{14}$, J. Solid State Chem. 228 (2015) 27–35, https://doi.org/10.1016/j.jssc.2015.04.016.

[5] Kahlenberg, The crystal structure of the strontium gallate $Sr_{10}Ga_6O_{19}$ and $Sr_3Ga_2O_6$, J. Solid State Chem. 160 (2001) 421–429, 10.1006/jssc.2001.9259.

[6] Chuer Hyun Moon, S.K. Singh, Dong Gi Lee, Soung Soo Yi, Kiwan Jang, Synthesis and optical characterization of novel $Sr_3Ga_2O_6$:Eu^{3+}, Ceram. Int. 38 (2012) 6789–6794, https://doi.org/10.1016/j.ceramint.2012.05.075.

[7] P S Anjana Revupriya, N. Gopakumar, M.S. Anju, Effect of Sr on the luminescence properties of Eu^{3+} activated xZnO(1-x)SrO-Al_2O_3 phosphors, Mater. Res. Express 7 (2020) 026203, https://doi.org/10.1088/2053-1591/ab771a.

[8] A. Luchechko, O. Kravets, L. Kostyk, O. Tsvetkova, Luminescence spectroscopy of Eu^{3+} and Mn^{2+} ions in $MgGa_2O_4$ spinel, Radiat. Meas. 90 (2016) 47–50, https://doi.org/10.1016/j.radmeas.2015.12.003.

[9] Yue Guo, Sung Heum Park, Byung Chun Choi, Hyun Jeong Jung, Jung Hwan Kim, Dual-mode manipulating multicenter photoluminescence in a single-phased $Ba_9Lu_2Si_6O_{24}$:Bi^{3+}, Eu^{3+} phosphor to realize white light/tunable emissions, Sci. Rep. 7 (2017) 15884, https://doi.org/10.1038/s41598-017-15903-7.

[10] Peipei Dang, Sisi Liang, Guogang Li, Wei Yi, Ziyong Cheng, Hongzhou Lian, Mengmeng Shang, Abdulaziz A. Al Kheraif, Jun Lin, Full color luminescence tuning in Bi^{3+}/Eu^{3+}- doped $LiCa_3MgV_3O_{12}$ garnet phosphors based on local lattice distortion and multiple energy transfers, Inorg. Chem. 57 (15) (2018) 9251–9259, https://doi.org/10.1021/acs.inorgchem.8b01271.

[11] Zhiguo Xi, Daimei Chen, Min Yang, Ting Ying, Synthesis and luminescence properties of YVO_4:Eu^{3+}, Bi^{3+} phosphor with enhanced photoluminescence by Bi^{3+} doping, J. Phys. Chem. Solid. 71 (2010) 175–180, https://doi.org/10.1016/j.jpcs.2009.10.016.

[12] N. Dhananjaya, H. Nagabhushana, B.M. Nagabhushana, S.C. Sharma, B. Rudraswamy, Synthesis, characterization, thermo- and photoluminescence properties of Bi^{3+} co-doped Gd_2O_3:Eu^{3+} nanophosphors, Appl. Phys. B 107 (2012) 503–511, https://doi.org/10.1007/s00340-012-4927-7.

[13] K. Lenczewska, Y. Gerasymchuk, N. Vu, N.Q. Liem, G. Boulonc, D. Hreniak, The size effect on the energy transfer in Bi^{3+} - Eu^{3+} co-doped $GdVO_4$ nanocrystals, J. Mater. Chem. C 5 (2017) 3014–3023, https://doi.org/10.1039/C6TC04660F.

[14] R.K. Rai, A.K. Upadhyay, R.S. Kher, S.J. Dhoble, Mechanoluminescence, thermoluminescence and photoluminescence studies on Al_2O_3:Tb phosphors, J. Lumin. 132 (2012) 210–214, https://doi.org/10.1016/j.jlumin.2011.08.003.

[15] Geetanjali Tiwari, Nameeta Brahme, Ravi Sharma, D.P. Bisen, Sanjay K. Sao, Ayush Khare, Fracto- mechanoluminescence and thermoluminescence properties of orange-red emitting Eu^{3+} doped $Ca_2Al_2SiO_7$ phosphors, J. Lumin. 183 (2017) 89–96, https://doi.org/10.1016/j.jlumin.2016.11.012.

[16] S. J Sajan, N. Gopakumar, P. S Anjana, R. S Kher, Revupriya, Synthesis, characterization and mechanoluminescence properties of europium doped (1-x) MgO.xBaO-Al_2O_3:0.1Eu (x = 0, 0.2,0.4,0.5,0.6,0.8 and 1.0) phosphor, Optik 156 (2018) 921–928, https://doi.org/10.1016/j.ijleo.2017.11.193.

[17] B. Vasanthi, N. Gopakumar, P.S. Anjana, Structural, optical and luminescence properties of $BaLaGa_3O_7$: xEu^{3+} ceramic phosphors, J. Lumin. 241 (2022) 118486, https://doi.org/10.1016/j.jlumin.2021.118486.

[18] B. Vasanthi, N. Gopakumar, P.S. Anjana, Girija Nair, Mechanoluminescence and photoluminescence properties of Eu^{3+} activated $SrGa_2O_4$ phosphors, Luminescence (2023) 1–11, https://doi.org/10.1002/bio.4602.

[19] Zhengwen Yang, Jiayan Liao, Shenfeng Lai, Hangjun Wu, Zezhi Fan, Jianbei Qiu, Zhiguo Song, Yong Yang, Dacheng Zhou, Energy transfer and photoluminescence properties in Bi^{3+} and Eu^{3+} co-doped ZnGa2O4, Mater. Express 3 (4) (2013) 350–354. https://doi:10.1166/mex.2013.1135.

[20] Rong Ying Liu, Yuan Zhang Feng, Zi Fei Peng, Impact of doping of Bi^{3+} on luminescent properties of red phosphors $Sr_{3-x}GaO_4F$:xEu^{3+}, Adv. Mater. Res. 1120 (2015) 401–405. https://doi:10.4028/www.scientific.net/AMR.1120-1121.401.

[21] V. Tsiumra, A. Krasnikov, S. Zazubovich, Ya Zhydachevskyy, L. Vasylechko, M. Baran, Ł. Wachnicki, L. Lipińska, M. Nikl, A. Suchocki, Crystal structure and luminescence studies of microcrystalline GGG:Bi3+ and GGG:Bi3+, Eu3+ as a UV-to-VIS converting phosphor for white LEDs, J. Lumin. 213 (2019) 278–289, https://doi.org/10.1016/j.jlumin.2019.05.034.

[22] Liang Zhang, Langping Dong, Yonghui Xu, Shuwen Yin, Hongpeng You, Site occupancy preference of Bi^{3+} and Bi^{3+}–Eu^{3+} codoped yttrium galliate phosphors for white LEDs, Dalton Trans. 50 (2021) 1366–1373, https://doi.org/10.1039/D0DT03983G.

[23] Lu Zheng, Dashuai Sun, Zeyu Lyu, Sida Shen, Pengcheng Luo, Shuai Wei, Luhui Zhou, Hongpeng You, Novel color tunable $LaCaGaO_4$:Bi^{3+}, Eu^{3+} phosphors for high color rendering warm white LEDs, J. Am. Ceram. Soc. 106 (11) (2023) 6617–6629, https://doi.org/10.1111/jace.19255.

[24] R.D. Shannon, C.T. Prewitt, Revised values of effective ionic radii, Acta Crystallogr. B26 (1970) 1046–1048, 10.1107/S0567740870003576.

[25] Shuxin Liu, Shuwei Ma, Shuxian Wang, Zhengmao Ye, Exploring crystal-field splittings of Eu^{3+} ions in γ- and β - $SrGa_2O_4$, J. Lumin. 210 (2019) 155–163, https://doi.org/10.1016/j.jlumin.2019.02.027.

[26] Xingyi Cai, Zhongfei Mu, Shaon Zhang, Daoyun Zhu, Qiang Wang, Yibin Yang, Dongxiang Luo, Fungen Wu, An investigation about the luminescence mechanism of $SrGa_2O_4$: Eu^{3+} showing no detactable energy transfer from the host to the dopant ions, J. Lumin. 200 (2018) 169–174. S1002-0721(10)60552-2.

[27] Chaochao Wang, Zhichao Liu, Alexey Nikolaevich Yakovlev, Tingting Hu, Tatiana Grigorievna Cherkasova, Xiaodie Zhu, Ya Liu, Jian Zhang, Daiyuan Liu, Xue Yu, Controlled mechano-luminescence properties of $SrGa_2O_4$:Tb^{3+} co-doping with Dy^{3+} and Eu^{3+} ions, RSC Adv. 13 (2023) 16405–16412, https://doi.org/10.1039/D3RA01985C.

[28] Ekta Rai, Ram Sagar Yadav, Dinesh Kumar, Akhilesh Kumar Singh, Vijay Janardhan Fulari, Shyam Bahadur Rai, Influence of Bi^{3+} ion on structural, optical, dielectric and magnetic properties of Eu^{3+} doped $LaVO_4$ phosphor, Spectrochim. Acta Mol. Biomol. Spectrosc. 243 (2020) 118787, https://doi.org/10.1016/j.saa.2020.118787.

[29] Minhee Noh, So-Hye Cho, Sangmoon Park, Tunable luminescence in Bi^{3+} and Eu^{3+} co-doped Sr_3AlO_4F Oxyfluorides phosphors, J. Lumin. 161 (2015) 343–346, https://doi.org/10.1016/j.jlumin.2015.01.046.

[30] R.S. Yadav, Dinesh Kumar, A.K. Singh, Ekta Rai, S.B. Rai, Effect of Bi^{3+} ion on upconversion-based induced optical heating and temperature sensing characteristics in the Er^{3+}/Yb^{3+} co-doped La_2O_3 nano-phosphor, RSC Adv. 8 (2018) 34699, https://doi.org/10.1039/c8ra07438k.

[31] M. Rai, S.K. Singh, K. Mishra, R. Shankar, R.K. Srivastava, S.B. Rai, Eu^{3+} activated $CaGa_2O_4$ wide band gap (WBG) material for solar blind UV conversion: fluorescence and photo-conductivity performance, J. Mater. Chem. (2) (2014) 7918–7926, https://doi.org/10.1039/C4TC00965G.

[32] X.Y. Liu, H. Guo, S.X. Dai, M.Y. Peng, Q.Y. Zhang, Energy transfer and thermal stability in Bi^{3+}/Eu^{3+} co-doped germanium-borate glasses for organic-resin-free UV LEDs, Opt. Mater. Express (2016) 3574, https://doi.org/10.1364/OME.6.003574.

[33] Vaibhav Chauhan, Prashant Dixit, Bi^{3+} assisted luminescence in $SrMoO_4$:Sm_{3+} red phosphors, J. Rare Earths 39 (11) (2021) 1336–1343, https://doi.org/10.1016/j.jre.2020.10.014.

[34] V.G. Suchithra, P. Prabhakar Rao, B.A. Aswathy, New full color emitting phosphor through energy transfer in Bi^{3+} and Eu^{3+} co-doped La_3TaO_7 weberite system, J. Mater. Sci. Mater. Electron. 31 (2020) 5141–5151, https://doi.org/10.1007/s10854-020-03074-7.

[35] Sun Qi, Thangavel Sakthivel, Balaji Devakumar, Shaoying Wang, Sanjay dhoble, Realizing bright blue-red color-tunable emissions from Gd_2GeO_5:Bi^{3+},Eu^{3+} phosphors through energy transfer toward light-emitting diodes, J. Lumin. 222 (2020) 117127, https://doi.org/10.1016/j.jlumin.2020.117127.

[36] Peng Du, Jae Su Yu, $Ba_3P_4O_{13}$:Eu^{3+} phosphors with high thermal stability and high internal quantum efficiency for near-ultraviolet white light-emitting diodes, Appl. Phys. A (2019), 10.1007/s00339-019-2395-1.

[37] S. J Sajan, N. Gopakumar, P. S Anjana, K. Madhukumar, Synthesis, characterization and mechanoluminescence of europium doped Zn(x)Ba(1-x)Al_2O_4 (x = 0, 0.4, 0.5, 0.6, 0.8, 1.0) phosphor, J. Lumin. 174 (2016) 11–16, 10.1016/j.jlumin.2016.01.024.

[38] Koen Binnemans, Interpretation of europium (III) spectra, Coord. Chem. Rev. 295 (2015) 1–45.

[39] Sanhai Wang, Yanqiao Xu, Ting Chen, Weihui Jiang, Jianmin Liu, Xin Zhang, Wan Jiang, Lianjun Wang, Bi^{3+} induced broad NUV-Excitation band in Eu^{3+} Doped red phosphor with scheelite-related structure, J. Lumin. (2019) 117019, https://doi.org/10.1016/j.jlumin.2019.117019.

[40] Kang Fengwen, Hu Yihua, Haoyi Wu, Guifang Ju, Zhongfei Mu, L.I. Nana, Luminescence investigation of Eu^{3+}-Bi^{3+} co-doped $CaMoO_4$ phosphor, J. Rare Earths 29 (9) (2011) 837–842, https://doi.org/10.1016/S1002-0721(10)60552-2.

[41] Jinfeng Lu, Zhongfei Mu, Daoyun Zhu, Qiang Wang, Fugen Wu, Luminescence properties of Eu^{3+} doped $La_3Ga_5GeO_{14}$ and effect of Bi^{3+} co-doping, J. Lumin. 196 (2018) 50–56, https://doi.org/10.1016/j.jlumin.2017.12.017.

[42] Lili Wang, Byung Kee Moon, Heum Park Sung, Hwan Kim Jung, Jinsheng Shi, Kwang Ho Kim Jung, Hyun Jeong, Synthesis and photoluminescence of Bi^{3+}, Eu^{3+} doped $CdWO_4$ phosphors an application of energy level rules of Bi^{3+} ions, New J. Chem. 40 (4) (2016) 3552–3560, https://doi.org/10.1039/c5nj03058g.

[43] Liang Jia, Liangling Sun, G. Annadurai, Balaji Devakumar, Shaoying Wang, Sun Qi, Jialei Qiao, Heng Guo, Bin Li, Xiaoyong Huang, Synthesis and photoluminescence characteristics of high color purity $Ba_3Y_4O_9$:Eu^{3+} red-emitting phosphors with excellent thermal stability for warm W-LED application, RSC Adv. 8 (2018) 32111–32118, https://doi.org/10.1039/C8RA06129G.

[44] Angel Morales Ramírez, Margarita García Hernández, Jonathan Yepez Ávil, Eu^{3+}, Bi^{3+} codoped Lu_2O_3 nanopowders: synthesis and luminescent properties, J. Mater. Res. 28 (10) (2013) 1365–1371, https://doi.org/10.1557/jmr.2013.91.

[45] Jianghui Zheng, Qijin Cheng, Zheng Cheng, Guo Chen, Feng Shi, Chao Chen, Correlated color temperature tunability and energy transfer phenomenon in the $NaBaBO_3$:Dy^{3+}/Eu^{3+} phosphor for white light applications, Funct. Mater. Lett. 8 (6) (2015) 1550077, https://doi.org/10.1142/S1793604715500770.

[46] Hekai Zhu, Zhiguo Xia, Haikun Liu, Ruiyu Mi, Zhuang Hui, Luminescence properties and energy transfer of Bi^{3+}/Eu^{3+}- codoped $Ca_{10}(PO_4)_6F_2$ phosphors, Mater. Res. Bull. 48 (2013) 3513–3517, https://doi.org/10.1016/j.materresbull.2013.05.045.

[47] Yao Wang, Ning Guo, Baiqi Shao, Congfei Yao, Ruizhuo Ouyang, Yuqing Miao, Adjustable photoluminescence of Bi^{3+} and Eu^{3+} in solid solution constructed by isostructural end components through composition and excitation-driven strategy, Chem. Engg. J. 421 (2) (2021) 127735, https://doi.org/10.1016/j.cej.2020.127735.

[48] Mariyam Thomas, Padala Prabhakar Rao, Sundaresan Pillai Kamalam Mahesh, Leela Sandhya Kumari, Peter Koshy, Luminescence properties of Eu^{3+}, Bi^{3+} co-activated $CaLaNbWO_8$ red phosphors under near UV and blue excitations, Phys. Status Solidi A 208. 9 (2011) 2170–2175, https://doi.org/10.1002/pssa.201026702.

[49] Hamdi Trabelsi, Marx Akl, Samer Hassan Akl, Ultrasound assisted Eu^{3+} doped strontium titanate nanophosphors: labeling agent useful for visualization of latent fingerprints, Powder Technol. 384 (2021) 70–81, https://doi.org/10.1016/j.powtec.2021.02.006.

[50] Shaobo Wang, Wenbo Chen, Dacheng Zhou, Jianbei Qiu, Xuhui Xu, Xue Yu, Long persistent properties of $CaGa_2O_4$:Bi^{3+} at different ambient temperature, J. Am. Ceram. Soc. 100 (2017) 3514–3521, https://doi.org/10.1111/JACE.14875.

[51] Huimin Li, Haiyan Wu, Ran Pang, Guanyu Liu, Su Zhang, Lihong Jiang, Da Li, Chengyu Li, Jing Feng, Hongjie Zhang, Investigation on the photoluminescence and thermoluminescence of $BaGa_2O_4$:Bi^{3+} at extremely low temperatures, J. Mater. Chem. C 9 (2021) 1786–1793, https://doi.org/10.1039/d0tc05122e.

[52] Peixin Gao, Qian Li, Siying Li, Shujie Gai, Yanan Li, Yibiao Ma, Zengtao Zhang, Mao Xia, Multiple strategies to approach high-efficiency luminescence controllable in blue/cyan/green-emitting Bi^{3+}-activated phosphors, J. Phys. Chem. C 126 (21) (2022) 9195–9206, https://doi.org/10.1021/acs.jpcc.2c02560.

[53] Hekai Zhu, Zhiguo Xia, Haikun Liu, Ruiyu Mi, Zhuang Hui Luminescence properties and energy transfer of Bi^{3+}/Eu^{3+}-codoped $Ca_{10}(PO_4)_6F_2$ phosphors, Mater. Res. Bull. 48 (9) (2013) 3513–3517, https://doi.org/10.1016/j.materresbull.2013.05.045.

[54] J.S. Revathy, Deepthi N. Rajendran, Temperature dependent photoluminescence studies of NUV excited Gd_2O_3: Eu phosphor, Mater. Today: Proc. 47 (9) (2021) 2007–2012, https://doi.org/10.1016/j.matpr.2021.04.161.

[55] Egle Ezerskyte, Julija Grigorjevaite, Sebastien Saitzek, Arturas Katelnikovas, Temperature-dependent luminescence of red-emitting $Ba_2Y_5B_5O_{17}$:Eu^{3+} phosphors with efficiencies close to unity for near-UV LEDs, Materials 13 (3) (2020) 763, https://doi.org/10.3390/ma13030763.

[56] Xin Zhang, Ruirui Cui, Jun Zhang, Xiaosi Qi, Chaoyong Deng, A novel red-emitting phosphor Ca_2GdNbO_6: Eu^{3+}: influences of sintering temperature and Eu^{3+} concentration on the photoluminescence, ECS J. Solid State Sci. Technol. 10 (2021) 026003, https://doi.org/10.1149/2162-8777/abe1d7.

[57] Liang Zhang, Yonghui Xu, Xiudi Wu, Shuwen Yina, Hongpeng You, Strong and pure red emitting Eu^{3+} doped phosphor with excellent thermal stability for warm LED's, Mater. Adv. 3 (2022) 2591, https://doi.org/10.1039/D1MA01221E.

[58] Zamin Khana Noor, Sayed Ali Khan, Li Zhan, Jalil Abdul, Jahangeer Ahmed, M. A. Majeed Khane, Muhammad Tahir Abbas, Feihong Wang, Xin Xu, Synthesis, structure and photoluminescence properties of Ca_2YTaO_6:Bi^{3+}/Eu^{3+} double perovskite white light emitting phosphors, J. Alloys Compd. 868 (2021) 159257, https://doi.org/10.1016/j.jallcom.2021.159257.

[59] Bao-Hua Di, Yu-Lan Chen, Recent progress in organic mechanoluminescent materials, Chin. Chem. Lett. 29 (2) (2018) 245–251, https://doi.org/10.1016/j.cclet.2017.08.043.

[60] Feng Ang, Philippe F. Smet, A review of mechanoluminescence in inorganic solids: compounds, mechanisms, models and applications, Materials 11 (4) (2018) 484, https://doi.org/10.3390/ma11040484.

[61] Ayush Kharea, B. Nag Bhargavi, Namrata Chauhan, Nameeta Brahme, Thermo and mechanoluminescence studies of BZT phosphor, Optik 125 (2014) 4655–4658, https://doi.org/10.1016/j.ijleo.2014.04.091.

[62] B.P. Chandra, V.K. Chandra, Jh Piyush, Models for intrinsic and extrinsic fracto-mechanoluminescence of solids, J. Lumin. 135 (2013) 139–153, https://doi.org/10.1016/j.jlumin.2012.10.009.

[63] Ravi Shrivastava, Jagjeet Kaur, Characterization and mechanoluminescence studies of $Sr_2MgSi_2O_7$:Eu^{2+}, Dy^{3+}, J. Rad. Res .Appl. Sci,. 8 (2015) 201–207, https://doi.org/10.1016/j.jrras.2015.01.005.

[64] Akshkumar Verma, Ashish Verma, Synthesis, characterization, mechanoluminescence, thermoluminescence, and antibacterial properties of $SrMgAl_{10}O_{17}$:Eu phosphor, J. Alloys Compd. 802 (2019) 394–408, https://doi.org/10.1016/j.jallcom.2019.06.209.

[65] Neha Tiwari, Raunak Kumar Tsmrakar, Mechanoluminescence, photoluminescence and thermoluminescence studies of $SrZrO_3$: Ce phosphor, J. Rad. res. Appl. Sci. 8 (2015) 68–76, https://doi.org/10.1016/j.jrras.2014.11.002.